Influence of grain size on the high-temperature creep behaviour of M5Framatome1 zirconium alloy under vacuum

G. Trego, J.C. Brachet, V. Vandenberghe, L. Portier, L. Gélébart, R. Chosson, J. Soulacroix, Samuel Forest, Anne-Françoise Gourgues-Lorenzon

Influence of grain size on the high-temperature creep behaviour of $M5_{Framatome}$[1] zirconium alloy under vacuum

G. Trego, J.C. Brachet, V. Vandenberghe, L. Portier, L. Gélébart, R. Chosson, J. Soulacroix, S. Forest, A.-F. Gourgues-Lorenzon

Abstract

The effect of grain size on the viscoplastic behaviour of $M5_{Framatome}$ zirconium alloy thin sheets was investigated at high temperature under uniaxial tension, using a variety of equiaxed microstructures with controlled grain sizes. In the α phase domain, a Coble diffusional creep regime and a dislocation creep regime were observed, in agreement with the literature. A negative sensitivity of the strain rate to temperature was highlighted in the upper part of the α+β two-phase temperature range, consistently with the literature. For the first time, a linear creep regime was evidenced in the β phase domain. In this regime, a sensitivity of the strain rate on the third power of the grain size is observed, suggesting a Coble regime with diffusion along grain boundaries.

Modelling with multi-mechanism Norton power-law rate equations, including dependence on grain size and a homogenous strain-rate assumption (Taylor model), enabled to satisfactorily reproduce the experimental results over the 700-1100 °C temperature range, especially the negative sensitivity of the strain rate to temperature between 880°C and 930°C. Very good agreement was obtained with a second order self-consistent and full field homogenization schemes.

1 Introduction

Zirconium alloys are widely used as cladding materials of nuclear fuel in light water reactors. Predicting their mechanical behaviour at high temperature is essential both to control manufacturing (hot forming) and to estimate their behaviour during postulated accident scenarios, such as loss-of-coolant accident (LOCA). These alloys exhibit two crystal structures according to temperature: hcp α phase at lower temperatures and bcc β phase at higher temperatures. According to the amount of alloying elements, significant amounts of both phases can coexist in a broad temperature range, typically, from 750-800 to 950-1000 °C (e.g. [Dupin et al 1999, Toffolon-Masclet et al. 2008]).

In the single-phase domains, the high-temperature viscoplastic flow behaviour of zirconium alloys is generally satisfactorily described by simple power-law (so-called Norton) equations, which are associated to dislocation climb as the rate controlling mechanism [Hayes & Kassner 2006][Charit & Murty 2008][Kaddour et al. 2004]. However, an unusual inverse temperature dependence of the strain rate has been highlighted in the two-phase α+β domain under low

[1] M5 and $M5_{Framatome}$ are trademarks or registered trademarks of Framatome or its affiliates, in the USA or other countries.

stress levels, yet without definitive experimental evidence of underlying physical mechanisms up to now [Kaddour et al. 2004, Massih 2013]. The contribution of grain size in the α+β domain was taken into account in [Massih 2013]; yet, as detailed below, experimental evidence, in particular close to the full β domain, is still missing. The present work aimed at addressing this issue.

To investigate the influence of grain size on viscoplastic flow in **α or near-α microstructures** (i.e., containing a small amount of β phase particles), authors generally compared data from materials having different grain sizes, but also different origins.

- In the high stress regime, a power-law dependence of creep rate on applied stress was reported, with no significant influence of the grain size for zirconium [Ardell 1964, Bernstein 1967, Warda et al 1973, MacEwen et al 1981, Prasad et al 1989, Prasad et al 1992, Rama Rao 1998] as well as for Zircaloy-4 [Donaldson & Ecob 1985].
- For lower applied stresses, a linear creep regime was reported except for very coarse-grained zirconium [Ardell 1964]. It was still observed for grain sizes as high as 50 µm [Bernstein 1967]. The finer the grain size, the higher the creep rate [Malakondaiah et al 1982, Donaldson & Ecob 1985]. Both the dependence on grain size and the values of activation energy suggested a Coble diffusional creep regime [Fiala & Čadek 1985, Fiala et al. 1991a-b, Prasad et al (1989, 1992), Rama Rao (1998), Kombaiah & Murty 2015a-b, Campello et al. 2017, Yadav et al. 2018] except when intermetallic precipitates decorated grain boundaries [Prasad 1989]. Diffusional flow was confirmed by transmission electron microscopy observations in the case of Zircaloy-4 [Kombaiah & Murty 2015b]. The boundary between high-stress and low-stress regimes was fully consistent with that published by [Sargent & Ashby (1982)].
- For higher grain sizes (typically, higher than about 100 µm), a low-stress Harper-Dorn viscous glide regime was also identified [Novotny et al 1985, Prasad et al 1989, 1992, Rama Rao 1998, Hayes & Kassner 2002, Pérez-Prado et al 2005, Hayes & Kassner 2006].

Almost all of these materials were obtained by cold deformation (rolling, drawing) followed by annealing. However, only a few studies addressed grain sizes close to that of industrial nuclear fuel cladding alloys, typically, about 5 µm, and even less addressed Zr-Nb alloys [Kombaiah & Murty 2015a].

In the **single-phase β domain**, only a dislocation creep regime has been reported in literature with a stress exponent in the range 3.2-4.3 [Ardell 1964, Abramyan et al 1967, Rose and Hindle 1973 and 1977, Hardy 1973, Clendening 1975, Hunt and Foote 1977, Burton et al. 1978, Clay and Stride 1978, Rizkalla et al 1979, Rosinger et al 1979, Shewfelt et al 1984, Stephan et al 1992, Fréchinet 2001, Kaddour 2004, Kaddour et al 2004, Rodchenkov and Semenov 2005, Charit and Murty 2008, Alymov et al 1987]. Namely, as for titanium alloys, β grain growth is fast in zirconium alloys, preventing from testing purely β microstructures with a rather fine grain size. Consequently, no correlation between the β grain size and the viscoplastic behaviour has been reported to the authors' knowledge.

Correlations between grain size and viscoplastic behaviour have only scarcely been reported in the **(α+β) phase domain**. Attention was mainly paid to the superplastic deformation regime by using processing maps associated with microstructural observations [Lee and Backofen 1967, Chung et al 1977, Singh et al 1993, Fotedar et al 1997, Shukla et al 1999, Hill et al 2001, Singh et al. 2001, Kapoor et al 2005, Saboori et al 2017, Sarkar et al 2017, Saxena et al 2018]. The reported stress exponent close to 2 suggests deformation by grain boundary sliding and typical strain rates involved in this regime range from 10^{-4} to 10^{-3} s^{-1}.

The increase, then decrease in creep rate of Zr-2.5%Nb under uniaxial tension, respectively reported between 750 °C and 850 °C, and between 850°C and 950°C, was attributed by Shewfelt et al. either to a change in grain size in the two-phase domain [Shewfelt at al 1984], or to a transformation-induced plasticity effect [Shewfelt & Lyall 1985]; nevertheless, no microstructural observations were reported to support the proposed mechanisms. A similar increase in creep rate was reported by [Hunt and Foote 1977, Alymov et al. 1987, Fréchinet 2001, Kaddour 2004, Jailin et al. 2020] close to the (α+β) / β phase boundary, i.e., in the upper part of the two-phase range, which will be denoted as "near-β" hereafter. At low stresses, a stress exponent close to 2 was reported in zirconium alloys [Clendening 1975, Hunt and Foote 1977, Rosinger et al 1979]. The high-stress regime was characterised by a stress exponent of up to 6 [Hunt and Foote 1977, Adam et al 1985 1987 1988 1989], suggesting dislocation creep.
On the basis of literature data, an inverse dependence of creep rate on the grain size was pointed out under low stresses, suggesting an Ashby-Verrall creep regime [Hayes and Kassner 2002, Pérez-Prado et al. 2005, Hayes and Kassner 2006, Kassner et al. 2007, Massih 2013]. Such an effect was much weaker in the dislocation creep regime observed under higher stresses. Hunt and Foote [1977] reported similar observations on Zr-2.5%Nb: they attributed the apparent negative sensitivity of strain rate to temperature to coarsening of the β phase, close to the upper boundary of the two-phase temperature range. However, to the authors' knowledge, neither systematic study nor experimental evidence of the effect of the size of β grains on the viscoplastic behaviour of zirconium or zirconium alloys in the upper part of the α+β temperature range have been reported yet.

The purpose of the present study was to systematically investigate the influence of grain size on the viscoplastic flow, for the $M5_{Framatome}$ cladding alloy, in both "near-α", (α+β) and "near-β" temperature ranges, and to represent experimental data by simple analytical modelling. To this aim, environmental effects were discarded by using a high vacuum creep facility as in [Fréchinet 2001, Kaddour 2004, Kaddour et al 2004, Kaddour et al 2011]. Indeed, oxygen uptake induces changes in phase equilibrium, as well as in mechanical properties at high temperature (e.g. [Chosson et al. 2016]); these effects were not considered in the present work. The grain size of both α and β phases were quantitatively related to the viscoplastic behaviour. A Zr-1%NbO chemistry was selected because it allows easy recognition of untransformed α grains and parent β grains after cooling down to room temperature. In contrast to Zircaloy-4, this chemistry allows decomposition of β grains into a lamellar microstructure for β grain size higher than about 15 µm at cooling rates close to a few degrees per second [Kaddour et al 2011]. On the basis of these experimental results, an improved constitutive model, which accounts for inverse temperature dependence of viscoplastic flow, is then proposed.

2 Materials and experimental procedures

2.1 Materials

In this work, 1.18-mm-thick sheet samples of $M5_{Framatome}$ alloy were used. Their typical chemical composition (in weight %) was: 1% Nb, 0.14% O and 0.035% Fe, bal. Zr. The as-received microstructure was fully recrystallized with equiaxed α grains of 6.3±0.5 µm in average size (Fig. 1a) and fine β_{Nb} particles inside the α grains.

In the present work, only temperatures higher than the monotectoid ($\alpha + \beta_{Nb} \rightarrow \alpha + \beta_{Zr}$) phase transformation point were considered (i.e., T > 600°C). Moreover, above the monotectoid temperature, but below the bulk transformation from α to β (i.e., for 600°C < T < ~800°C), a few per cents of β_{Zr} phase were present as discrete precipitates inside α grains and along α grain boundaries. This low fraction of β precipitates did not strongly affect the creep behaviour at high temperature [Charit and Murty 2008]. Additionally, intragranular intermetallic Nb and Fe-rich precipitates were also still present in this temperature range, but their fraction was very limited (<<1%), most of them increasingly dissolved with increasing high-temperature creep exposure and those precipitates may not contribute to the overall mechanical behaviour of the cladding in the conditions of interest for this work. Thus, in the following, the small fraction of monotectoid β_{Zr} and intermetallic particles is not explicitly considered. This microstructure will be termed "near-α" hereafter.

In order to investigate the effect of grain size in the near-α and β phase domains, model microstructures were prepared using dedicated thermal-mechanical treatments. As for the near-α domain, as-received sheets were further cold-rolled to thicknesses of 0.91 mm and 0.76 mm respectively, then annealed in secondary vacuum at 700 °C for 16 h. They were then polished and etched as described in Section 2.3. The resulting model materials still possessed a recrystallized near-α microstructure with α grain sizes d_α of 9.1±0.5 µm and 7.6±0.5 µm, respectively (Figs 1b, 1c). The crystallographic textures of the reference and near-α model materials were typical of recrystallized Zr-Nb alloys, with basal poles tilted by 22-27° from the normal direction toward the transverse direction of the sheet.

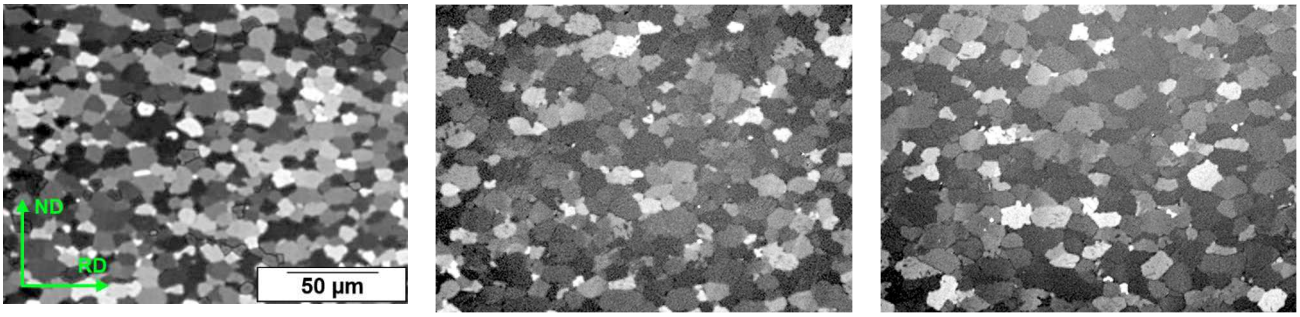

a) $d_\alpha \approx 6.3$ µm b) $d_\alpha \approx 7.6$ µm c) $d_\alpha \approx 9.1$ µm

Figure 1: Optical micrographs (polarised light, "Nomarski" contrast) of as-received $M5_{Framatome}$ and "near-α" model materials with various average α grain sizes, d_α – RD: rolling direction, ND: normal direction to the sheet plane. Same magnification and sample orientation for the three micrographs.

Properly assessing the gain size effect in the β domain requires hindering β grain growth, which is ordinarily very rapid in zirconium alloys. Pinning β grain boundaries by a low fraction of α phase particles was reported to limit grain growth in the near-β temperature range [Langeron & Lehr 1959, Nowikov & Pfeiffer 1957, Sills & Holt 1979, Hunt & Foote 1977]. This approach was used in the present study to obtain microstructures with controlled β grain size. The model microstructures were created by applying heat treatments to the as-received materials right before starting the creep test, without in-between return to low temperature (the thermal cycles are depicted as insets in Fig. 2). The creep specimens were hold for 30 min in the near-β phase domain (900 to 930 °C) or in the single-phase β domain

(960 °C) to set the β grain size before going back to the creep testing temperature, namely, 900°C (Fig. 2). The specimens were hold for 30 min at 900°C before starting the creep test. The fraction of β phase present during the creep test was determined using resistivity measurements (see Section 2.2.) during stress-free holding at 900°C. Corresponding values are also indicated in Fig. 2. As in [Kaddour et al 2011], no further microstructural modifications were expected during creep. Consequently, only *post-mortem* microstructures, obtained after preliminary heat treatment + creep + final cooling, are shown in the following.

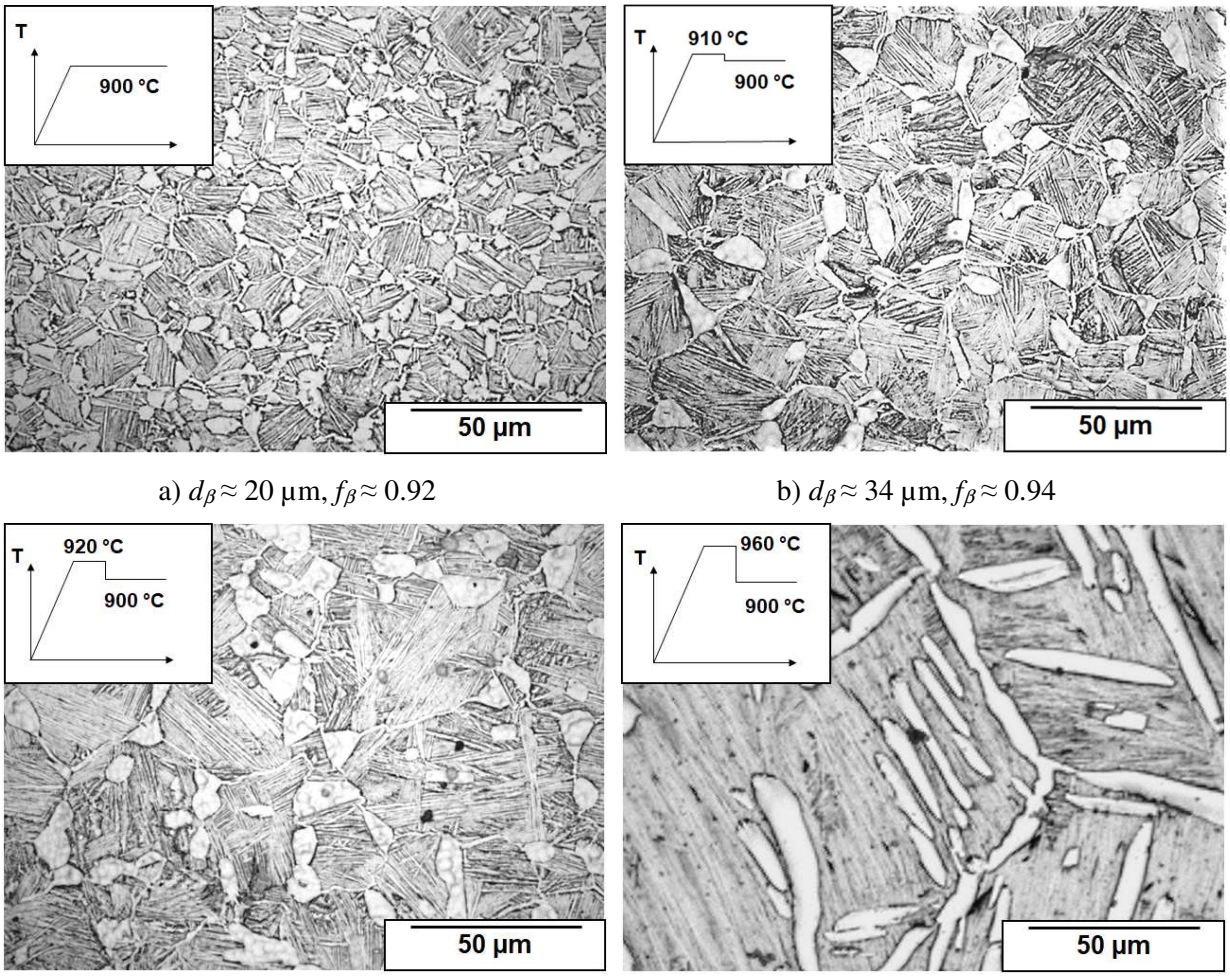

a) $d_\beta \approx 20$ µm, $f_\beta \approx 0.92$ b) $d_\beta \approx 34$ µm, $f_\beta \approx 0.94$

c) $d_\beta \approx 48$ µm, $f_\beta \approx 0.96$ d) $d_\beta \approx 595$ µm, $f_\beta \approx 0.92$

Figure 2: Optical micrographs of "near-β" model materials with various average β grain sizes, d_β, and fractions of β phase, f_β after cooling down to room temperature (insets: thermal cycles involving the short holding at high temperature followed by the isothermal creep test). Bright regions: α phase; grey, lath-like or acicular regions: as-quenched β phase. Note that the α phase observed in (d) was formed during final interrupted cooling and was not present during the creep test.

2.2 Creep tests

Isothermal creep tests were conducted in secondary vacuum, by applying a tensile load along the rolling direction of the sheets. The testing facility was similar to that detailed in [Kaddour et al 2011]. The load was measured with accuracy better than 0.7 N using a 500 N load cell. A radiation furnace was used to apply controlled thermal cycles to full-thickness dogbone

specimens having a gauge length of 18 mm and a gauge width of 3 mm. The distance between specimen ends (including fillets) was 30 mm. The temperature was controlled with accuracy better than 0.6 % using an S-type thermocouple spot-welded on the central part of the specimen. The thermal gradient was measured to be ±5 °C in the gauge region and post-test observations confirmed that microstructures were homogeneous all along the gauge part of the specimens. Including the 6 mm-long fillets on both sides of the gauge part, the thermal gradient was close to 20°C. As in [Kaddour et al 2011], phase transformations were continuously monitored using four-point potential drop (resistivity) measurements with a typical accuracy of ±5 %. This method had previously been validated by comparison with calorimetric experiments, image analysis, calculated equilibrium phase diagrams based on a modified version of the Zircobase® database [Dupin et al 1999], and kinetics calculations [Kaddour et al 2004]. In the present case, all experimental methods used for phase quantification gave very similar results (Fig. 3). As already mentioned, in the low-temperature domain (between 600 and ~800°C), the small fraction of β phase was not explicitly considered in the present study, even if it was present in the microstructure and predicted in equilibrium calculations. Fig. 3 also shows that for the as-received material, the α grain size remained constant all over the near-α domain and even in the (α + β) phase domain, whereas the β grain size sharply increased with temperature in the (α + β) domain.

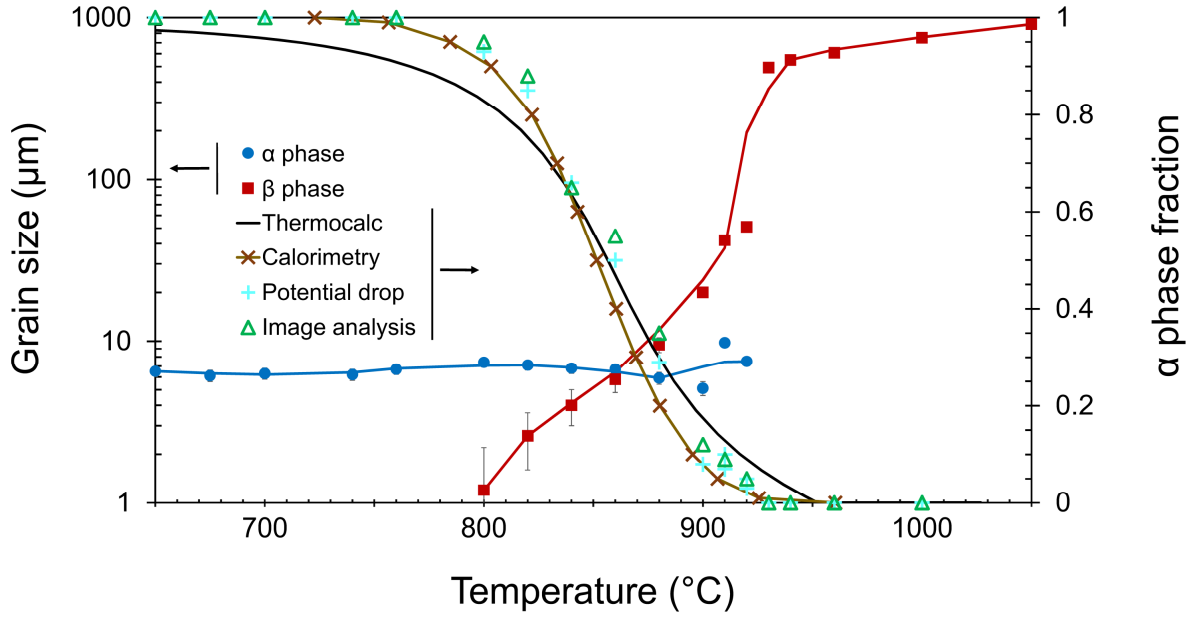

Figure 3: α-phase fraction, using various experimental methods and equilibrium predictions (Thermocalc), and average grain size as a function of temperature – As-received material. Thermocalc data are taken from [Dupin et al. 1999]. Calorimetry, potential drop and image analysis data are taken from [Kaddour et al. 2004].

Before applying the tensile load, all creep specimens were hold for 30 min at the creep test temperature in order to stabilise their microstructure. More precisely:

- In the near-α domain, no significant microstructural evolution was expected to occur;
- In the (α+β) and near-β domains, phase fractions and grain sizes were expected to stabilise before application of load;
- In the β domain, stabilisation of the β grain size was expected during holding.

Several constant load levels were then applied in turn to the same specimen, as in [Fréchinet 2001, Kaddour 2004, Kaddour et al 2004, Kaddour et al 2011]. Each load level was applied for an amount of time such that the increase in strain was close to 2% for that level. The true stress was calculated from the length and section area data corresponding to the midpoint of the considered load level, by assuming no volume change in the gauge part of the specimen. The true strain rate was calculated by determination of the slope of the true strain vs. time curve for the considered load level. The absence of any load history effect was checked for each test by increasing, then decreasing the load levels. The difference between two successive load levels being small, no primary creep was observed at all. Steady-state deformation occurred right after having reached the new load level. Creep test conditions are summarised in Table 1. Unless otherwise stated, only one test was performed for each condition, the reproducibility of results having been checked during previous studies [Kaddour 2004, Kaddour et al 2011]. To facilitate identification of the β phase that was present during the creep tests, the specimens were cooled at 5 °C.s^{-1} after creep, leading to a Widmanstätten-like or acicular microstructure of the quenched prior-β phase (Fig. 2). After creep in the fully β domain, cooling was interrupted by an isothermal loading at 880°C for 30 min to precipitate intergranular α phase that delineated β grain boundaries (Fig. 2d).

Two methods were used for monitoring elongation of the gauge part during the creep tests. Elongation of the sole gauge part was monitored by the already mentioned four-point potential drop method. A more direct, contactless laser extensometer method was also used to monitor the distance between specimen ends; the actual initial value of this distance (close to 30 mm) was measured with an accuracy of ±13 µm. The data provided by extensometer measurements were first processed to get a *first estimate* of strain rate as a function of applied stress. To estimate the strain, the measured elongation was divided by a reference gauge length. To this aim, two assumptions were made in turn; (i) only the gauge part of the specimen was actually deformed (reference gauge length: 18 mm); (ii) both the gauge part and the fillet were uniformly deformed (reference gauge length: 30 mm). Assumption (i) tends to overestimate strains, then strain rates, whereas assumption (ii) tends to strongly underestimate them. Assumption (i) was reasonable in most cases. As will be shown below, the stress sensitivity of viscoplastic flow was significant, especially in the high-stress regime where the stress exponent was much larger than 1. As the stress level was lower in the fillets than in the gauge part, the contribution of fillets to total elongation was expected to be weak whatever the testing conditions. Moreover, the temperature was slightly lower in the fillets than in the gauge region, which also tends to lower the contribution of fillet deformation to total elongation in most testing conditions.

To *refine* strain measurements, an iterative method based on three-dimensional finite element simulations with Cast3m [Cast3m] of the whole specimen was used for each temperature, to identify the parameters of a constitutive model (see Section 4). The full set of data points obtained from the two assumptions was used to initialize the constitutive parameters using a least squares method. Excellent agreement was obtained between experimentally measured displacement vs. time curves and those predicted by the model. In the following, only the curves obtained using each temperature-specific constitutive model parameters will thus be displayed to represent laser extensometer measurements.

As will be further discussed below, in the 900-940 °C temperature range, the peculiar viscoplastic behaviour of zirconium alloys, characterized by an inverse sensitivity of the strain rate to temperature and a stress exponent close to 1, prevent from neglecting elongation of the

yet cooler fillets in extensometer data processing. As a result, only results from the potential drop method were considered in this temperature range.

As previously mentioned, for any of the creep test conditions considered in this work, no transient (primary) creep was observed, so that only steady-state values of strain rate will be considered in the following.

Table 1: Summary of creep tests performed in the present study. Values indicated in parentheses are those for "model" microstructures with controlled grain size. One specimen per condition except for tests denoted with an asterisk (two tests per condition, three tests at 960°C)

Domain	Near-α					α + β				
Test temperature (°C)	650	675	700	740	760	800	820	840	860	880
Range of true stress (MPa)	1-80	1-50	1-46 (1-60)	1-45	1-30	1-20	1-20	1-20	1-15	1-15
Domain	Near- β					β				
Test temperature (°C)	900	910	920	930	940	960	1000	1050		
Range of true stress (MPa)	1-12 (1-10)	1-10*	1-7*	1-7*	1-8*	1-8*	1-5*	1-4.6*		

2.3 Microstructure observations and analysis

Microstructural observations were conducted after conventional polishing. Grain size determination was carried out by separately considering α and β phases.

In the near-α phase domain, namely, for temperatures lower than 800°C (Table 1), a specific etching procedure was used. The α grain size was quantified by automated processing of optical micrographs taken with "Nomarski" contrast. An in-house imaging processing program was adapted to that purpose. More than 3000 grains per sample were measured, for an untested reference sample and for each tested microstructure.

For α+β, near-β and fully-β microstructures, samples were etched in a solution composed of 5 mL hydrofluoric acid, 50 mL nitric acid and 45 mL glycerol before observation by optical microscopy. Parent β grains were manually identified from the morphology of Widmanstätten-like colonies obtained after final cooling. Equiaxed (see Figs 2-(a), (b) and (c)) regions were considered as untransformed α phase. After manual identification of boundaries, grain sizes were measured by automated image analysis using ImageJ® software. For the (α+β) microstructures, phase fractions were extracted and about 100 grains of each phase were quantified. Owing to their coarser grain size, only 50±10 grains were analysed for each sample in the near-β and fully-β microstructures.

3 Experimental results and discussion

3.1 Viscoplastic behaviour of the as-received material

3.1.1 Near-α domain

Viscoplastic strain rate vs. stress curves, as well as power-law exponents are reported in Fig. 4a for near-α microstructures. First, very satisfactory agreement was obtained between extensometer and potential drop measurement methods. These results on flat specimens also closely agree with those reported on as-received (tubular) fuel claddings tested in the same facility [Kaddour et al 2011], with a difference in strain rates lower than 50 % at a given stress level. In agreement with many literature data, two creep regimes were observed in the near-α domain, namely, a linear creep regime at low stresses (< 15 MPa) and a power-law creep regime at high stresses. The intermediate stress regime with power-law exponent close to 3, sometimes reported in Nb-containing Zr alloys [Murty et al 1995, Murty et al 2005, Charit and Murty 2008, Zhou et al 2004, Kombaiah & Murty 2015a], was not clearly evidenced here and will not be further discussed. Apparent activation energies for each regime are reported in Fig. 5. They were significantly higher than those reported in [Kaddour et al 2011], respectively, 133 kJ/mol and 194 kJ/mol in the low-stress and high-stress regimes. Yet, the temperature range investigated here was rather narrow (110°C) so that the uncertainty on the values of activation energies is probably rather high. The present values were also higher than those reported in literature in the low-stress creep regime of Zr-Nb alloys, namely, 107-137 kJ/mol [Murty et al 2005, Zhou et al. 2004]. Literature data on activation energies in the high-stress regime are scattered (244-402 kJ/mol) [Murty et al. 1995, Murty et al 2005, Charit and Murty 2008, Zhou et al 2004, Kutty et al 1997, Hayes & Kassner 2006] but encompass the value found in the present work (250 kJ/mol).

a)

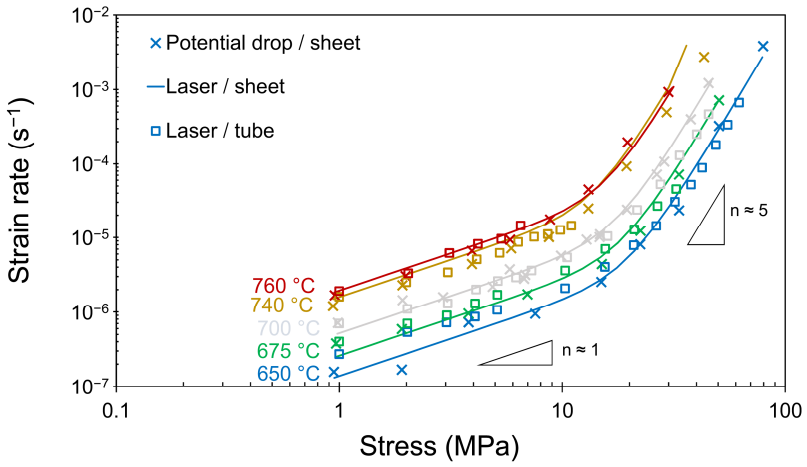

b)

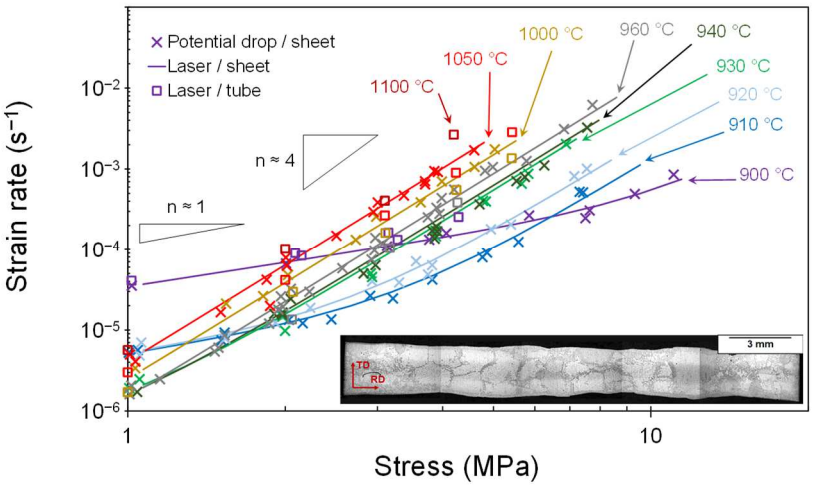

Figure 4: Strain rate as a function of stress and temperature in a) the near-α domain and b) in single-phase β and in the upper part of (α + β) domains. Sheet data from the present work, as-received material, "tube" data from fuel claddings with similar microstructure [Kaddour et al. 2011] – Inset in b): optical micrograph of a sheet specimen after creep at 1050 °C and cooling down to room temperature.

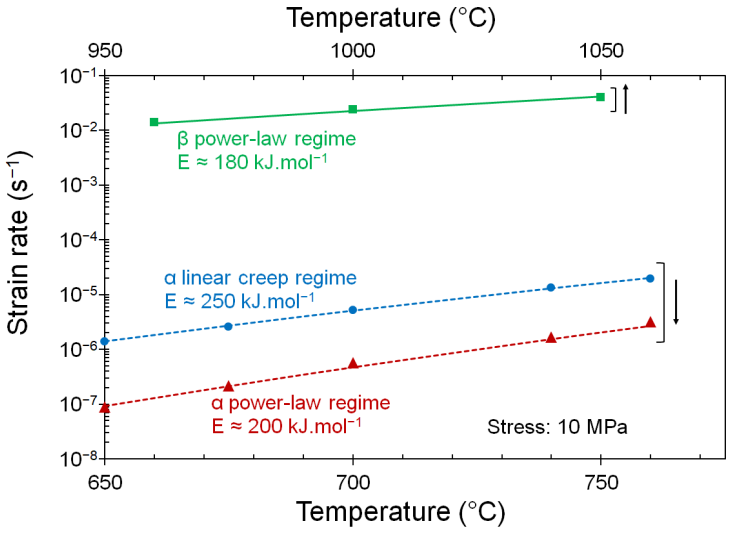

Figure 5: Apparent activation energy determined for each creep regime in the near- α domain (temperatures along lower X-axis) and in the single-phase β domain (temperatures along upper X-axis)

3.1.2 Near-β domain (900-930°C) and single-phase β domain (930-1100°C)

Creep results in these domains are reported in Fig. 4b. As shown in Fig. 2, the β grain size of many of these creep specimens was very coarse. Consequently, only 2-3 grains were present across the thickness of the specimens. As a consequence, deformation was rather heterogeneous on a grain-by-grain basis, as shown in the inset of Fig. 4b. For this reason, several tests were conducted per condition but macroscopic strain rate vs. stress data still were

very reproducible from one test to another. In this temperature range, the results were also very close to those reported by [Kaddour et al 2011] on claddings, also plotted in Fig. 4b.

Two power-law regimes are evidenced in Figure 4b, with a smooth transition between them, in the lower part of this temperature range. The extent of the "low exponent" regime was broader for lower test temperatures. It was hardly visible at 930 °C and disappeared at higher temperatures. This extent can be correlated to the smaller β grain size (Fig. 3) due to pinning by the low fraction of untransformed α particles (6-8 % at 900-940 °C, Fig. 2 and Fig. 3). To confirm this result and to check the influence of the β grain size on the viscoplastic behaviour in this "near-β" temperature range, tests were carried out at constant temperature, on "model" materials with controlled β grain size.

One characteristic feature of the unusual behaviour in the "near-β" temperature range was that for lower stress levels, the sensitivity of strain rate to temperature was much lower (and even strongly negative between 900°C and 910°C) than for higher stress levels, where only the high-exponent regime was found.

3.1.3 Two-phase (α + β) domain (800-920°C)

Creep data in the (α + β) temperature range, with significant fractions of the two phases, are reported in Fig. 6a. Again, potential drop and laser extensometer measurements were in close agreement to each other, and the results were similar to those reported for claddings in [Kaddour et al 2011]. A low-stress regime was clearly identified, with a power-law exponent of 1.3. This value is higher than those reported for Coble creep (close to 1) but lower than those reported for grain boundary sliding (close to 2). At higher stresses, the dependence of strain rate on applied stress appeared higher but no power-law regime could be unambiguously identified. In fact, strain rates were as high as 10^{-3} s^{-1} for stresses close to the upper bound of the low-stress regime, around 20 MPa. In the low-stress regime, creep results are summarised in Fig. 6b over the entire range of tested temperatures and microstructures. Only the 1-4 MPa stress range is represented in Fig. 6b for clarity. The β grain size and fractions of α phase are also recalled in Fig. 6b. Corresponding microstructures are reported in Fig. 7. Two behaviours clearly appeared in the range 800-900°C:

- From 800 to 860°C: (α + β) microstructures with a majority of connected α phase exhibited a positive sensitivity of viscoplastic strain rate to temperature, with higher flow rates at higher temperatures, under given stress. The size of α grains was essentially unchanged (Fig. 2, Figs 7a-d) whereas that of β grains increased with temperature but remained fine (up to 6.4 µm, Fig. 6b, Figs 7a-d). The creep strength decreased with increasing f_β, suggesting that the β phase was weaker than the α phase.
- From 860 to 900°C (extending the temperature range investigated by [Kaddour et al 2011]): these microstructures possessed a higher fraction of connected β phase and exhibited an inverse sensitivity to temperature in this low-stress regime, with a power-law exponent of about 1.5.

These data agree with the already reported sensitivity of creep rate to temperature in the upper part of the two-phase domain of zirconium alloys [Hunt and Foote 1977, Alymov et al. 1987, Fréchinet 2001, Kaddour 2004, Jailin et al 2020]. In the present work, the link with microstructure was further investigated by considering grain size effects, which are reported in the next section.

a)

b)

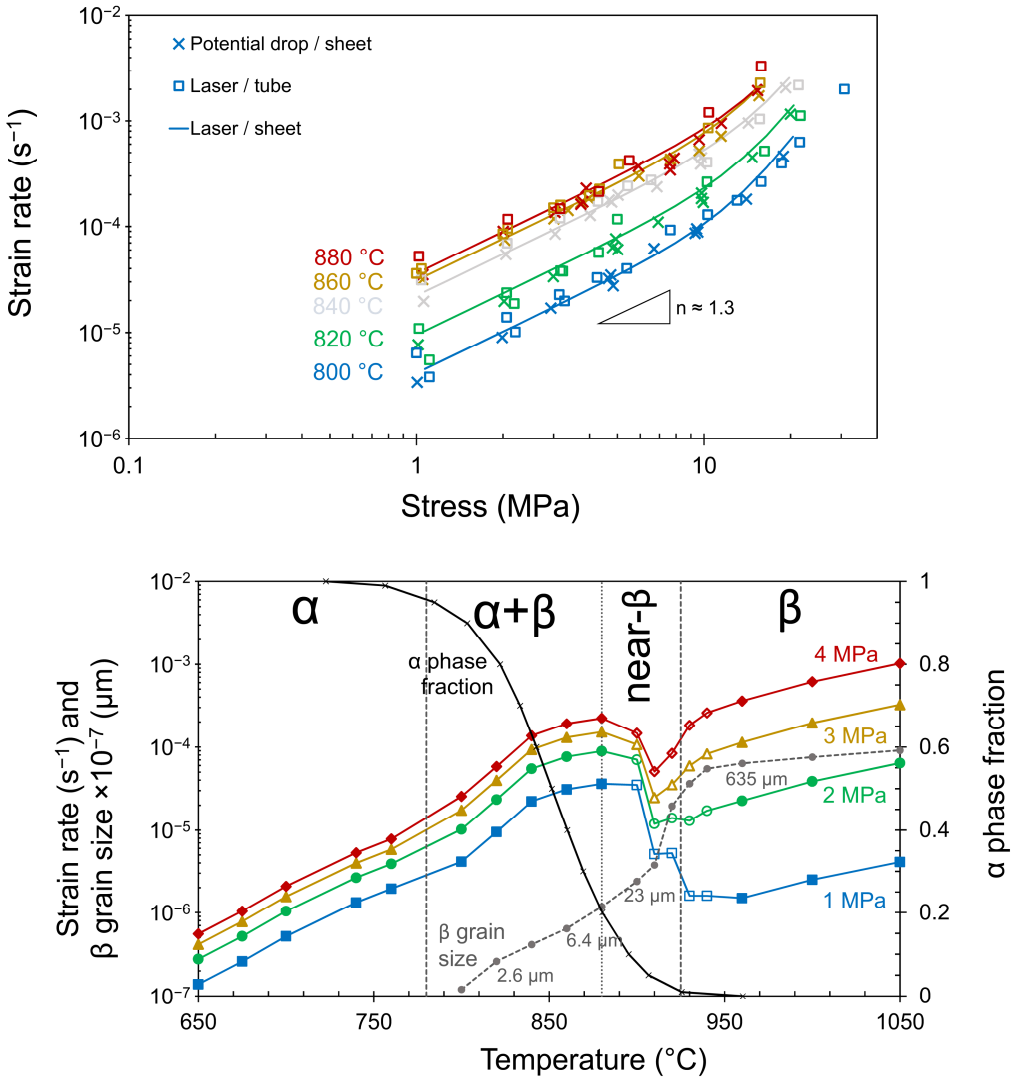

Figure 6: Strain rate a) as a function of stress in the (α+β) domain and b) as a function of temperature from 650 to 1050 °C, plotted together with the α phase fraction (right vertical axis) and the β grain size (left vertical axis) – Axial creep tests on as-received $M5_{Framatome}$ sheet (this work) and cladding tube samples [Kaddour et al 2011].

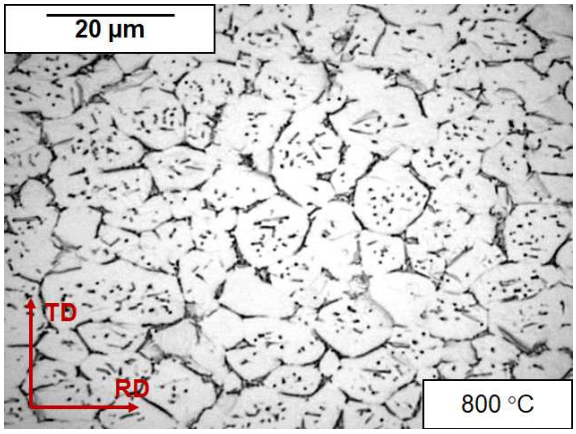

a) $f_\beta \approx 0.07$

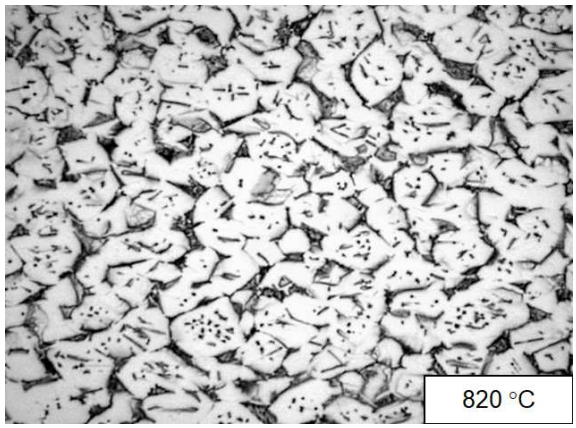

b) $f_\beta \approx 0.15$

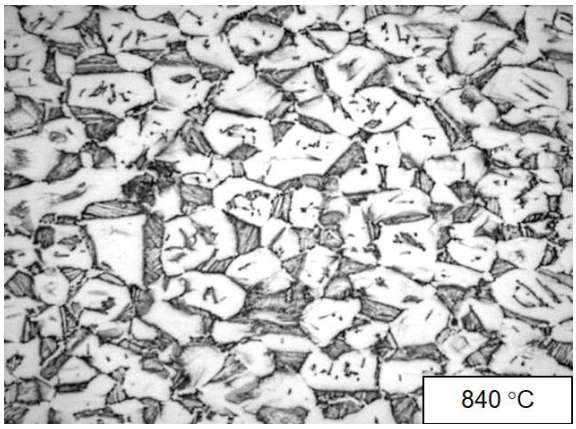

c) $f_\beta \approx 0.34$

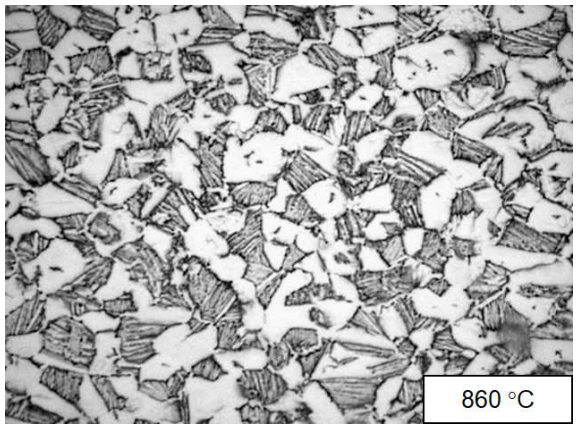

d) $f_\beta \approx 0.50$

e) $f_\beta \approx 0.74$

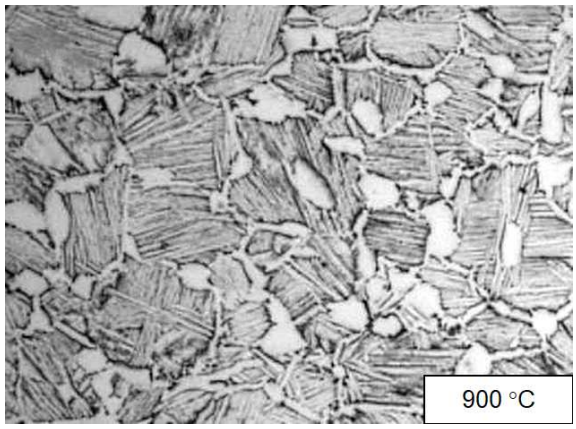

f) $f_\beta \approx 0.92$

Figure 7: Optical micrographs of as-received material specimens after creep tests in the (α + β) domain, from 800 to 900 °C – Same magnification for all micrographs.

3.2 Effect of grain size on the viscoplastic flow in the near-α and near-β domains

3.2.1 Near-α domain

From the Norton plots of Fig. 8a, both high-stress and low-stress creep regimes were found with similar stress exponents whatever the α grain size, d_α. Figure 8 also evidences an effect

of grain size in the low-stress creep regime as already reported in literature (see Introduction). This suggests that the underlying deformation mechanism might be due to diffusional flow (Coble or Nabarro-Herring regime) rather than to viscous glide (Harper-Dorn regime). The narrow range of investigated grain sizes does not allow accurate determination of the grain size dependence from the present experimental results. Nevertheless, from Fig 8b, the strain rate seems to more closely linearly depend on the reverse third power than on the reverse square of grain size. Even if the morphology of the α phase is complex in the present case, this suggests a Coble diffusional creep regime, as already pointed out for pure zirconium and for zirconium alloys [Fiala & Čadek 1985, Fiala et al. 1991a-b, Prasad et al 1989, Prasad et al 1992, Rama Rao 1998, Kombaiah & Murty 2015a-b, Campello et al. 2017, Yadav et al. 2018].

a)

b)

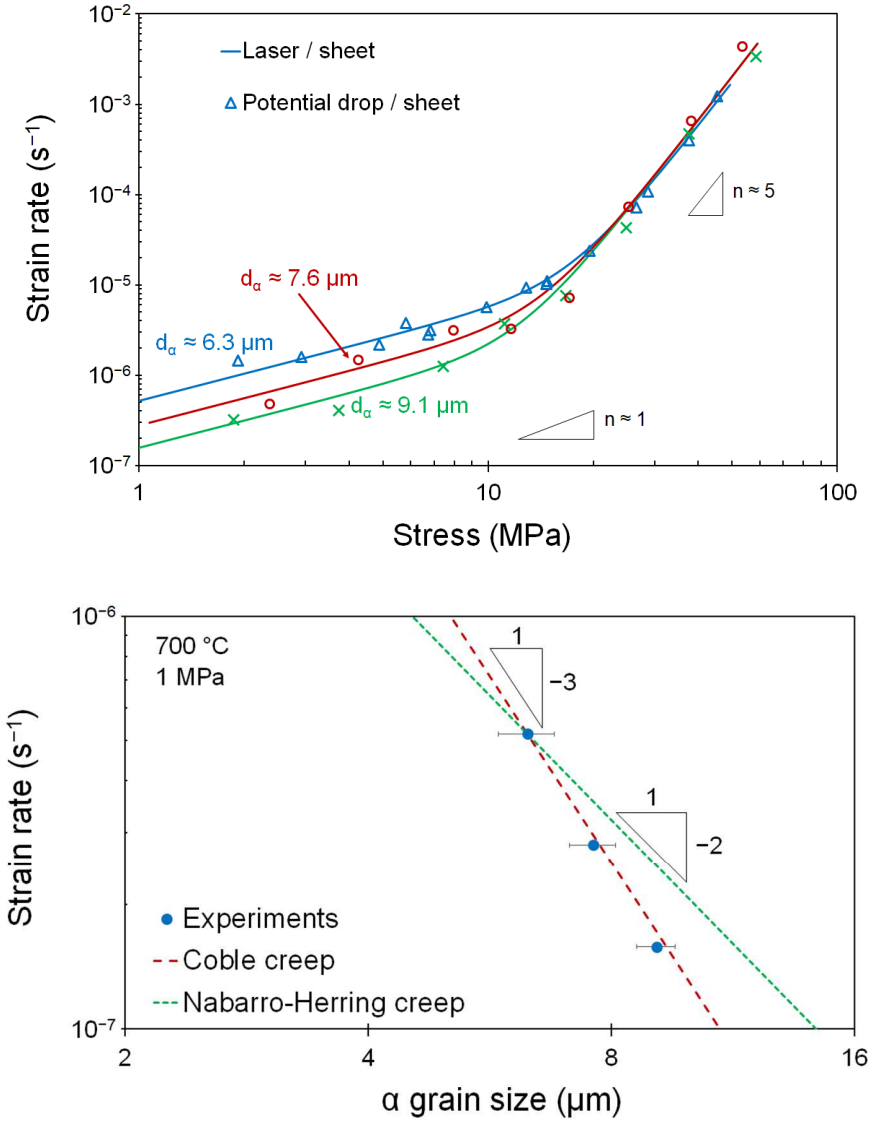

Figure 8: Strain rate at 700 °C as a function of a) the axial stress and b) the α grain size under 1 MPa (logarithmic scales) – Axial creep tests on flat specimens made of as-received $M5_{Framatome}$ and "near-α" model materials.

3.2.2 Near-β domain

For the first time, for the near-β domain, Norton plots of Fig. 9a show that both high-stress and low-stress creep regimes actually exist, the latter for β grain sizes, d_β lower than 34 µm. This regime is also suggested at lowest strain rates for d_β = 48 µm, but it was not observed for the coarser grain size (d_β = 595 µm). As already discussed, in this temperature range, the fraction of α phase did not exceed 8% and the α phase was present as discrete particles. Consequently, this phase was not expected to govern the creep regime and its contribution to the creep behaviour in this domain was not explicitly considered. Thus, only the effect of the β grain size will be discussed here. Fig. 9b illustrates the effect of d_β in each of the two regimes. Fig. 9 shows a limited, but non-negligible effect of d_β in the high-exponent creep regime, with apparent exponent of grain size close to 2. A similar effect was already reported by [Shahinian and Lane 1953] for a Ni-Cu alloy, by [Garofalo 1964] for an austenitic steel, by [Petkovic et al. 1979] for Cu and by [Kassner & Li 1992] for pure Al; yet, to the authors' knowledge, it has never been reported for Zr alloys and more generally, for bcc alloys. This will be further interpreted using a Hall-Petch treatment in the Modelling section.

a)

b)

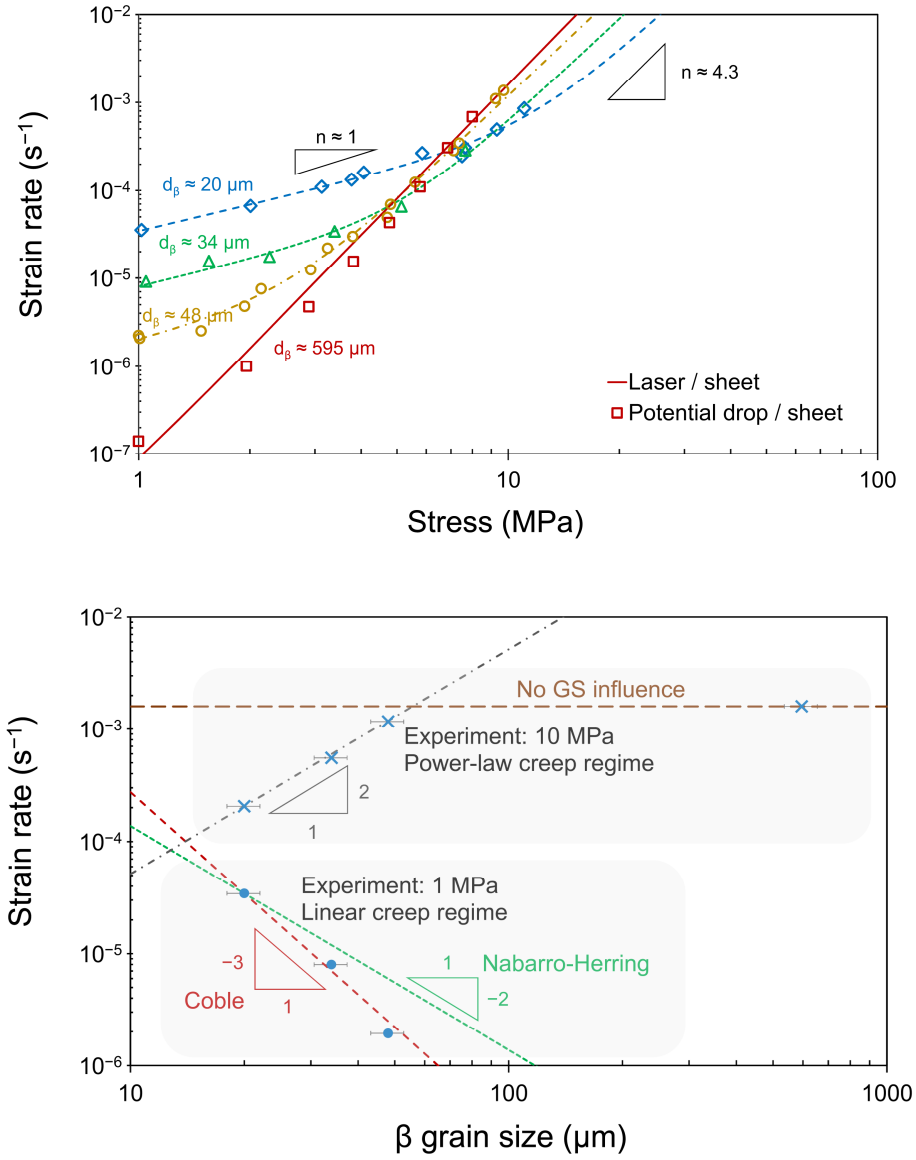

Figure 9: Strain rate at 900 °C as a function of a) the axial stress and b) the β grain size under 1 MPa (low stress regime) and 10 MPa (high stress regime) – As-received $M5_{Framatome}$ (d_β = 595 µm) and "near-β" model materials.

Figure 9 also evidences a strong effect of d_β in the low-stress creep regime, together with a stress exponent close to 1. Even if only three values of d_β were tested, Fig. 9b suggests a dependence of the strain rate on the reverse third power of d_β. The accuracy of grain size exponent was better than for the near-α domain due to the broader range of investigated values of d_β and to more limited evolution of grain shape and topology with temperature. These results strongly suggest a Coble diffusional creep regime in this temperature and stress range.

To summarise experimental data, creep regimes and corresponding parameters of interest are reported in Table 2.

Table 2: Creep regimes and corresponding parameters experimentally determined in the present work.

Temperature range	Near-α (650-760°C)		α + β (800-880°C)		Near-β (900-930°C)		β (930-1000°C)
Stress regime	Lower (1-10 MPa)	Higher (20-80 MPa)	Lower (< 10 MPa)	Higher (> 10 MPa)	Lower (a few MPa)	Higher (close to 10 MPa and above)	Only one regime observed
Stress exponent	1	5	1.3	≈4	1	≈4	≈4
Apparent activation energy (kJ/mol)	250	200	no simple dependence on temperature				180

4 Viscoplastic constitutive modelling including grain size effects

4.1 Constitutive equations of α and β phases

In the following, all tensors are denoted in **bold** characters. Due to the strong crystallographic texture of the starting materials, and to the orientation relationships between the two phases, both α and β phases are potentially anisotropic in creep properties in the considered microstructures. Nevertheless, no data is available about such anisotropy in the high temperature range considered here. In the present work, an isotropic viscoplastic potential, using a Von Mises equivalent stress, σ_{VM}, together with the usual stress deviator, $\boldsymbol{\sigma^D}$, was adopted to represent the constitutive behaviour of each phase. Isotropic elastic moduli were also assumed. By considering the anisotropic mechanical behaviour of zirconium alloys, the present model coefficients are only relevant to the particular loading mode and material considered here, namely, uniaxial tension along the rolling direction of the sheet axis (or along the tube axis in [Kaddour 2011]), under secondary vacuum.

As the amount of strain experienced by specimens did not exceed a few per cents for each load level, a small strain assumption formulation was adopted in the modelling approach. For each phase, the total strain rate tensor was decomposed into three additive contributions by following Eq. (1):

$$\dot{\boldsymbol{\varepsilon}} = \dot{\boldsymbol{\varepsilon}}^{\boldsymbol{el}} + \dot{\boldsymbol{\varepsilon}}_{\boldsymbol{l}}^{\boldsymbol{vp}} + \dot{\boldsymbol{\varepsilon}}_{\boldsymbol{h}}^{\boldsymbol{vp}} \quad (1)$$

In Eq. (1), $\dot{\boldsymbol{\varepsilon}}^{\boldsymbol{el}}$ is the elastic strain rate tensor, determined using Hooke's equation; $\dot{\boldsymbol{\varepsilon}}_{\boldsymbol{l}}^{\boldsymbol{vp}}$ is the contribution of viscoplastic flow in the "low-stress" (Coble) regime, and $\dot{\boldsymbol{\varepsilon}}_{\boldsymbol{h}}^{\boldsymbol{vp}}$ is the contribution of viscoplastic flow in the "high stress" (dislocation creep) regime.

The Young's modulus, *E*, of each phase was taken from [Darchis 1984] as a function of temperature. For the α phase, *E* (GPa) = 108.8 - 0.05475*T* and for the β phase, *E* (GPa) = 92.1 - 0.0405*T*, *T* being the absolute temperature. In view of the low stress values and of the slow evolution of true stress within a single load level, the contribution of the elastic strain rate to the total strain rate was negligible.

Rate equations for the α phase

The viscoplastic strain rate of the α phase in the "high-stress" regime was described by the normality rule together with a power-law equation as follows:

$$\dot{\boldsymbol{\varepsilon}}_{\boldsymbol{h}}^{\boldsymbol{vp}} = \frac{A_h}{T}\left(\frac{\sigma_{VM}}{\sigma_0}\right)^{n_h} exp\left(\frac{-Q_h}{RT}\right) \cdot \frac{3}{2}\frac{\boldsymbol{\sigma^D}}{\sigma_{VM}} \quad (2)$$

In Eq. (2), *T* is the absolute temperature, *R* is the gas constant, Q_h= 250 kJ/mol and n_h= 5 are respectively the apparent activation energy and the power-law exponent determined from experimental curves (Fig. 4 and Fig. 5) and A_h= 1.2×10^5 K·s^{-1} is an adjustable coefficient; σ_0 is a reference stress taken as 1 MPa. No effect of α grain size was introduced in the high-stress regime for the α phase, in accordance with the experimental results in the near-α domain. The effect of (minor) β_{Zr} phase particles was implicitly taken into account in the value of A_h.

The viscoplastic strain rate in the low-stress (Coble) regime was described by the normality rule together with a power-law equation as follows:

$$\dot{\boldsymbol{\varepsilon}}_{\boldsymbol{l}}^{\boldsymbol{vp}} = \frac{A_l}{T}\left(\frac{d_{ref}}{d}\right)^3\left(\frac{\sigma_{VM}}{\sigma_0}\right)^{n_l} exp\left(\frac{-Q_l}{RT}\right) \cdot \frac{3}{2}\frac{\boldsymbol{\sigma^D}}{\sigma_{VM}} \quad (3)$$

In Eq. (3), Q_l= 200 kJ/mol and n_l = 1 are respectively the apparent activation energy and the power-law coefficient determined from experimental curves (Fig. 4), and A_l = 2.7×10^7 K·s^{-1} is an adjustable coefficient. σ_0 was also taken as 1 MPa. d is the α grain size at the considered temperature and d_{ref} is a reference grain size, taken as that of the as-received material i.e. 6.3 µm. Note that the value of A_l is dependent of those taken for d_{ref} and σ_0.

Rate equations for the β phase

The contribution of the Coble regime was described using the same equation as for the α phase, namely, Eq. (3), but with different values of material parameters. The value of d_{ref} was set to 20 µm, close to the value of d_β at 900°C (Fig. 6b). The values of Q_l= 450 kJ/mol, n_l= 1 and A_l= 4.5×10^{18} K·s^{-1} were determined from experimental data. Note that to be fully consistent with the Coble creep regime assumption, the value of n_l slightly differs from that determined in Fig. 6a. The value of Q_l is surprisingly high but it was only identified over a very narrow temperature range (910-930°C) and no value is available from literature to make comparisons, so that the uncertainty is also very high.

In the high-stress regime, experimental observations also revealed an effect of grain size for moderate values of d_β (Fig. 9b). In the model, a Hall-Petch treatment of the flow stress was thus applied, for values of d_β lower than a threshold grain size, d_{th}. To this aim, it was

recalled that in the classical theory of plastic deformation, the contribution of grain size hardening to the yield stress is proportional to the inverse square root of the grain size. In the high-stress regime (dislocation creep), a similar contribution was assumed by considering the power-law dependence of strain rate on applied stress in the above Eq. (2). By inverting this equation, for given strain rate, $\dot{p}$, the flow stress is proportional to $\dot{p}^{1/n_h} {d_\beta}^{-1/2}$ so that the strain rate is proportional to the product ${\sigma_{VM}}^{n_h} {d_\beta}^{\frac{n_h}{2}}$. As the grain size dependence was much weaker between 50 µm and 595 µm (Fig. 9b), the threshold value was assumed to be closer to 50 µm than to 500 µm. The value of d_{th} was determined from the tests in the near-β and β domains and it was set to 90 µm. Its exact value did not significantly influence model predictions. Taking the grain size into account resulted in the following equation (4) for the high stress regime in the β phase:

$$\dot{\boldsymbol{\varepsilon}}_{\boldsymbol{h}}^{\boldsymbol{vp}} = \frac{A_h}{T} \cdot \left[min\left(1, \frac{d_\beta}{d_{th}}\right)\right]^{\frac{n_h}{2}} \cdot \left(\frac{\sigma_{VM}}{\sigma_0}\right)^{n_h} exp\left(\frac{-Q_h}{RT}\right) \cdot \frac{3}{2} \frac{\boldsymbol{\sigma^D}}{\sigma_{VM}} \quad (4)$$

The values of Q_h= 180 kJ/mol, n_h= 4 and A_h= 7.1×10^4 K·s^{-1} were determined from experimental data (Fig. 4 and Fig. 5). Note that the value of $n_h/2$ = 2 is fully consistent with the effect of grain size reported in Fig. 9 in the considered regime.

The values of model parameters are summarised in Table 3.

Table 3: Viscoplastic model parameters. N/A: not applicable.

	Low-stress regime					High-stress regime				
Parameter	A_l	d_{ref}	n_l	Q_l	σ_0	A_h	d_{th}	n_h	Q_h	σ_0
Physical unit	K·s^{-1}	µm	-	kJ/mol	MPa	K·s^{-1}	µm	-	kJ/mol	MPa
α phase	2.7×10^7	6.3	1	200	1	1.2×10^5	N/A	5	250	1
β phase	4.5×10^{18}	20	1	450	1	7.1×10^4	90	4	180	1

4.2 Taking the two-phase microstructure into account using homogenisation models

Except for temperatures higher than 960 °C, there were two phases in the tested microstructures. Viscoplastic deformation might be decomposed into three main contributions:

- Deformation of the α phase, including contributions from dislocation creep (power-law) regime and from diffusional flow assisted by deformation at α grain boundaries (Coble regime).
- Deformation of the β phase, including contributions from dislocation creep (power-law) regime and from diffusional flow assisted by deformation at β grain boundaries (Coble regime).
- Deformation driven by diffusional flow and/or dislocation motion at α/β interphase boundaries.

In the simple approach reported here, only the first two contributions were explicitly considered, in spite of the high density of α/β interphase interfaces in the (α+β) microstructures. A mean field model was adopted by considering the α and β phases separately, based on well-known micromechanical theoretical schemes [Qu 2006]. Several homogenisation schemes were used to derive the relationship between "local" values (i.e., for each phase) and average values of stress and strain fields.

In the near-α domain, only the α phase was considered. It is first recalled that in this temperature range, fine Nb-rich β_{Nb} particles that were present in the initial microstructure had dissolved. As a consequence, this model cannot be directly extrapolated to lower temperatures, where these particles are still present and can strengthen the material. The remaining β_{Zr} phase particles were small, distributed in a non-continuous manner and their fraction did not exceed a few per cents. They were not expected to strongly affect viscoplastic flow mechanisms of the material. As a consequence, they were not explicitly taken into account in the model. Similarly, in the near-β domain, alpha particles were distributed at β grain boundaries, but in a very discontinuous manner (Fig. 2, Fig. 7f). They were also assumed to not strongly affect the average constitutive behaviour of the material, so that only the β phase was explicitly modelled.

In the (α+β) temperature range, three mean-field homogenisation schemes were considered. In all three methods, the plastic strain rate in each phase was computed from the corresponding stress values according to the homogenisation rules:

$$\dot{\boldsymbol{\varepsilon}}_{\boldsymbol{\alpha}} = \dot{\boldsymbol{\varepsilon}}_{\boldsymbol{l\alpha}}^{\boldsymbol{vp}} + \dot{\boldsymbol{\varepsilon}}_{\boldsymbol{h\alpha}}^{\boldsymbol{vp}} \text{ and } \dot{\boldsymbol{\varepsilon}}_{\boldsymbol{\beta}} = \dot{\boldsymbol{\varepsilon}}_{\boldsymbol{l\beta}}^{\boldsymbol{vp}} + \dot{\boldsymbol{\varepsilon}}_{\boldsymbol{h\beta}}^{\boldsymbol{vp}} \quad (5)$$

where indices *l* and *h* respectively refer to the distinct flow rules for low and high stress loading.

The overall stress and strain rates were computed as averages of the corresponding values in the phases:

$$\boldsymbol{\Sigma} = \left(1 - f_{v\beta}\right)\boldsymbol{\sigma}_{\boldsymbol{\alpha}} + f_{v\beta}\boldsymbol{\sigma}_{\boldsymbol{\beta}} \text{ and } \dot{\boldsymbol{E}} = \left(1 - f_{v\beta}\right)\dot{\boldsymbol{\varepsilon}}_{\boldsymbol{\alpha}} + f_{v\beta}\dot{\boldsymbol{\varepsilon}}_{\boldsymbol{\beta}} \quad (6)$$

The concentration (resp. localisation) rules indicate how the mean stress (resp. strain) in each phase is computed from overall quantities. They differ in the three homogenisation methods used in the present work:

- The *iso-strain rate (Taylor-like) model* enforces the fact that both phases are subjected to the same overall strain rates:

$$\dot{\boldsymbol{E}} = \dot{\boldsymbol{\varepsilon}}_{\boldsymbol{\alpha}} = \dot{\boldsymbol{\varepsilon}}_{\boldsymbol{\beta}} \quad (7)$$

  which corresponds to the homogeneous strain rate assumption. The stress values in the individual phases are obtained from the overall stress by numerically solving the system of two nonlinear equations, namely, equation (5) and the left part of equation (6), taking equation (7) into account.

- In contrast, the *iso-stress (Sachs) model* considers that the stress is homogeneous in the composite material as in the following equation (8):

$$\boldsymbol{\Sigma} = \boldsymbol{\sigma}_{\alpha} = \boldsymbol{\sigma}_{\beta} \tag{8}$$

  For a prescribed overall tensile stress, the resulting strain rate is computed by combining equations (5) and the right part of equation (6) after enforcing the previous iso-stress conditions.

- The *second order self-consistent estimate* proposed by [Ponte Castaneda 2002a, 2002b] is an extension of the variational self-consistent model by the same author. It provides estimates of the second moment of the stress distribution, i.e., the variance of stress values in individual phases. This is in contrast to earlier generalizations of the self-consistent homogenization scheme, which concentrate on the evaluation of the first moment, i.e., the average stress in each phase. It turns out that this procedure also provides more accurate estimates of the effective viscoplastic behaviour of composites; see the discussion in [Brenner et al. 2004] and more recently [Pilvin, Onimus et al. 2017]. The numerical implementation used in the present work is due to [Castelnau et al. 2008].

The iso-strain rate and iso-stress models provided bounds for the effective viscoplastic dissipation potential. In the case of creep loading conditions, the iso-stress (resp. iso-strain rate) models generally provide an upper (lower) bound in terms of resulting strain rate. This is, however, not always the case when several mechanisms are considered in the individual phases (two viscoplastic strain rates with distinct power laws in each phase, as presented in section 4.1), see [Trego 2011]. The second order self-consistent estimate is generally bounded by the iso-strain rate and iso-stress predictions.

The predictions of the previous mean field models have been compared to full-field finite element simulations taking the morphology of the phases explicitly into account. Realistic finite element meshing techniques of the microstructure were presented in [Trego 2011] comparing usual Voronoi tessellation and more sophisticated representations of the microstructure. These simulations did not significantly improve the predictions. That is why they are not detailed here for the sake of conciseness. Some of these intensive computational results are used as validations for the previous mean field estimates. For that purpose, various boundary conditions were applied to statistical elementary volumes (SEV) containing Voronoi tessellation with random distribution of the phases among the cells with prescribed overall volume fraction:

- HSBC: homogeneous stress boundary conditions;
- HDBC: homogeneous deformation boundary conditions;
- PBC: periodic boundary conditions.

The reader is referred to [Kanit et al. 2003] and [Trego 2011] for the accurate description of these boundary conditions and of their implementation for creep loading in the finite element code Cast3m.

It should be pointed out that the constitutive behaviour of Zr-Nb alloys is very sensitive to their microstructure [Kaddour et al 2011], so that the present model is only intended to be relevant to more or less equiaxed microstructures. It cannot be applied to acicular or basketweave microstructures resulting from the decomposition of the β phase during cooling (Fig. 2, Fig. 7).

4.3 Comparison between experimental data and model predictions

From model predictions in the near-α and (near-β and β) temperature ranges, constitutive equations appeared to satisfactorily describe the average viscoplastic behaviour of each phase under uniaxial tension, as shown in Figure 10.

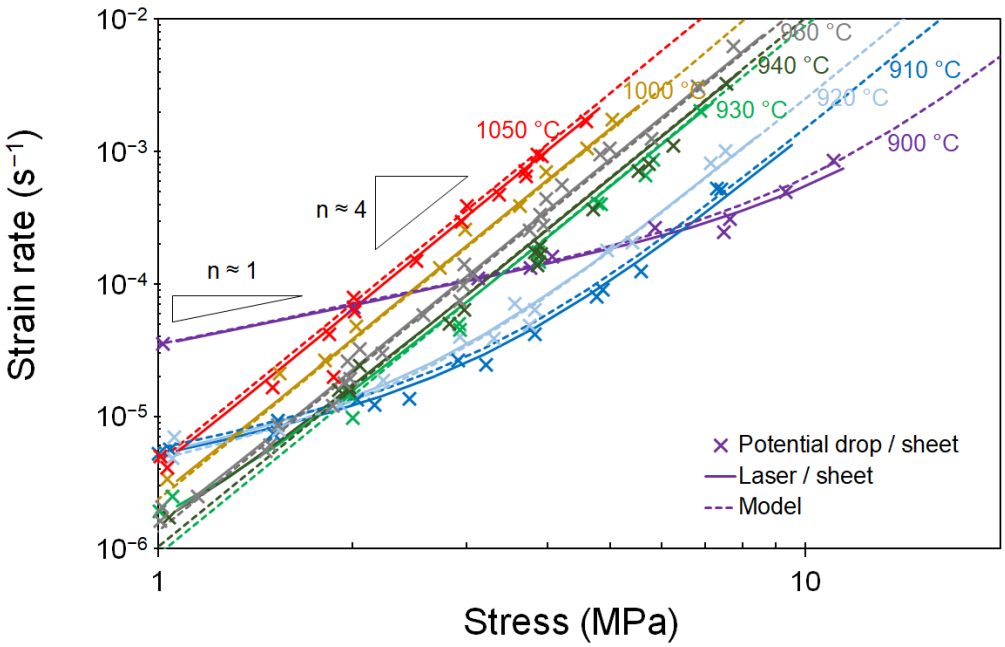

Figure 10: Strain rate as a function of the axial stress – Model predictions and axial creep tests on flat specimens made of as-received $M5_{Framatome}$ and "near-β" model materials.

The model predictions and experimental results are now compared in the (α + β) temperature range. Fig. 11 shows the predicted and experimentally measured overall strain rates as a function of the applied stress at six different temperatures from 800 to 900°C. The iso-stress and iso-strain rate estimates were found to be upper and lower bounds of the experimental values in the considered range of stress and temperature. The experimental results were found to be closer to the iso-strain rate estimate in general.

The predictions of the second order self-consistent scheme and of the finite element simulations are compared with the experimental results in Fig. 12a at the creep testing temperature of 860°C. A remarkable agreement is observed showing the accuracy of the second order estimate supported by the full field simulations using PBC. Full field simulations with PBC also provided excellent estimates of the effective behaviour over the whole temperature range 800-900°C, as demonstrated by Fig. 12b, for a low stress value. The stress-based and strain-based boundary conditions predicted strain rates which were respectively closer to the iso-stress and to the iso-strain rate model estimates. These results demonstrate the accuracy of the two-regime viscoplastic model identified for the individual phases; they also demonstrate that homogenisation methods can be used in the future to explore the material response for other loading conditions.

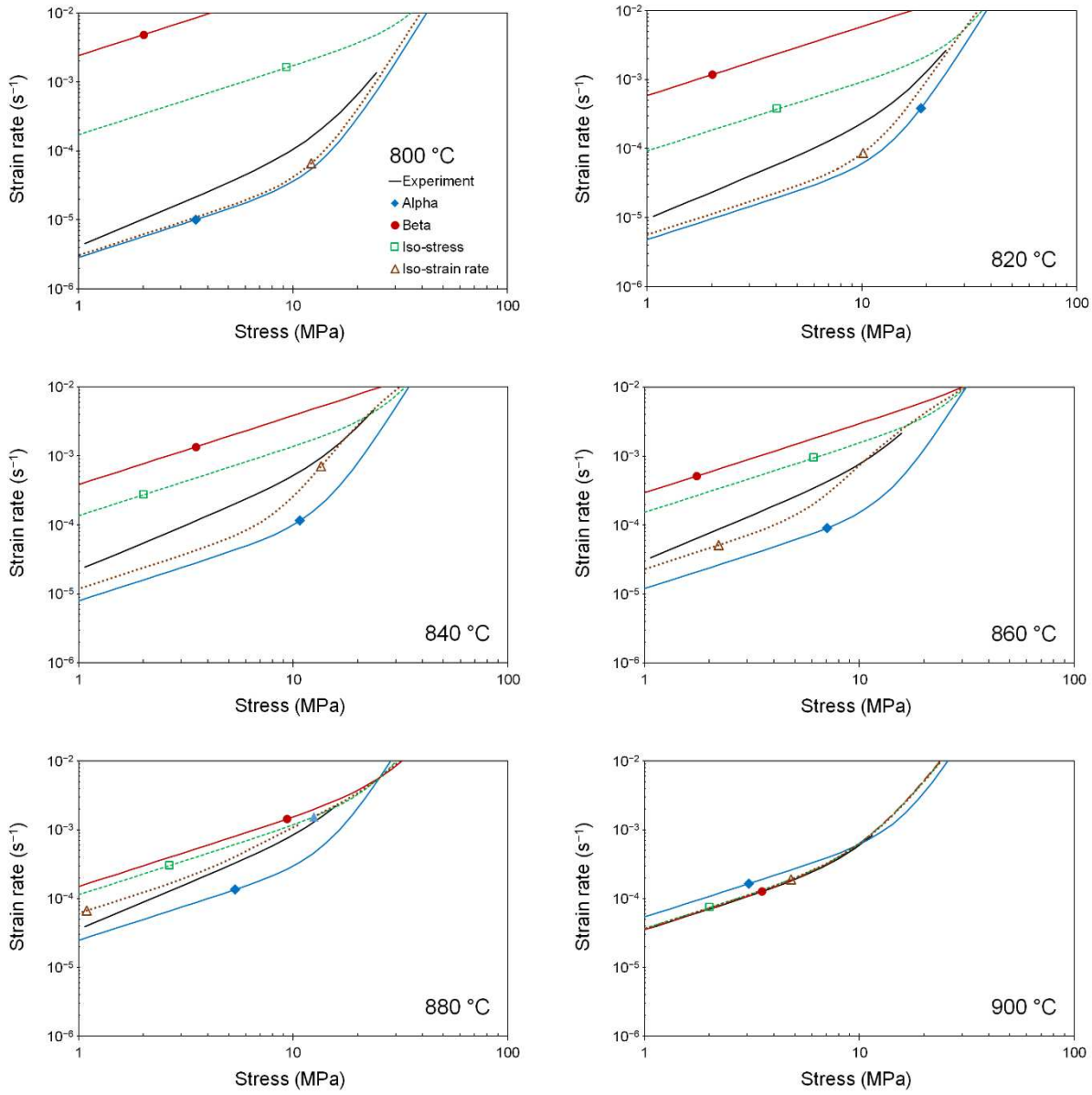

Figure 11: Strain rate as a function of stress, from 800 to 900 °C, experimental results on $M5_{Framatome}$ flat specimens, predictions from single-α and single-β creep flow equations and from iso-stress and iso-strain rate homogenisation models.

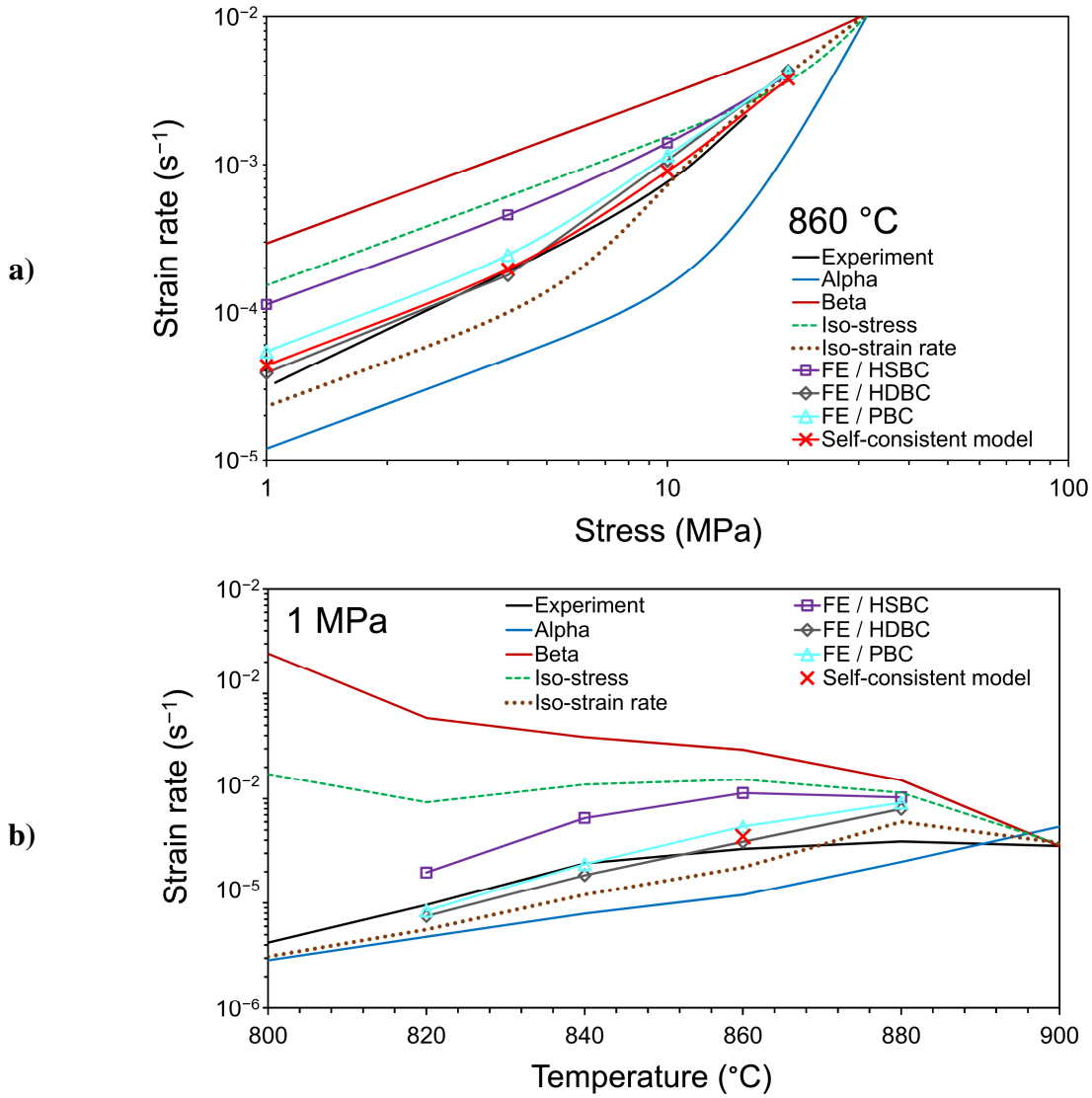

Figure 12: a) Strain rate as a function of a) stress at 860 °C and b) temperature under 1 MPa – Experimental results on $M5_{Framatome}$ flat specimens, predictions from single-α and single-β creep flow equations, from iso-stress and iso-strain rate homogenisation models, and average predictions from FE simulations on SEV with various boundary conditions and from the self-consistent model. The reader is referred to Section 4.2 for the meaning of abbreviations.

The approach developed by Massih [Massih 2013] was based on the Ashby-Verrall regime; even if an inverse square dependency of strain rate on grain size was present in the rate equation, Massih assumed a constant grain size over the entire (α+β) temperature range. Note that no result between 900°C and 960°C was available from the experimental database [Kaddour et al 2004] that was used to adjust model parameters in [Massih 2013]. As a result, a positive sensitivity of viscoplastic strain rate to temperature was predicted by this model even over the near-β temperature range.

On the other hand, the present phenomenological model actually takes the grain size into account; as a consequence, it describes enhanced viscoplastic flow in this temperature range very satisfactorily. This phenomenon is attributed to the particular microstructure exhibiting

both fine α and fine β grains. Yet, a limit of the present model is that diffusional flow at interphase interfaces is not explicitly taken into account. It is only implicitly represented using the fine grain size and a Coble-like regime for both phases. As viscoplastic flow in this material strongly depends on its microstructure [Kaddour et al 2011], the present model parameters are only relevant to equiaxed microstructures with the considered texture.

By using both experimental results and model predictions, a deformation-mechanism map was built as in [Kaddour et al 2004] but with modelling over the whole temperature range (Fig. 13). This map allows satisfactory description of the viscoplastic behaviour of the alloy. Its validity is limited to rather low stresses and low to moderate strain rates; on the other hand, the viscoplastic behaviour is described with a unique model and set of constitutive parameters, provided that the grain size of each phase is entered at each considered temperature. To obtain a fully continuous model, the evolution of grain size with temperature should be described by using analytical equations (possibly fitted on more complex modelling such as phase-field approaches). This is out of scope of the present study.

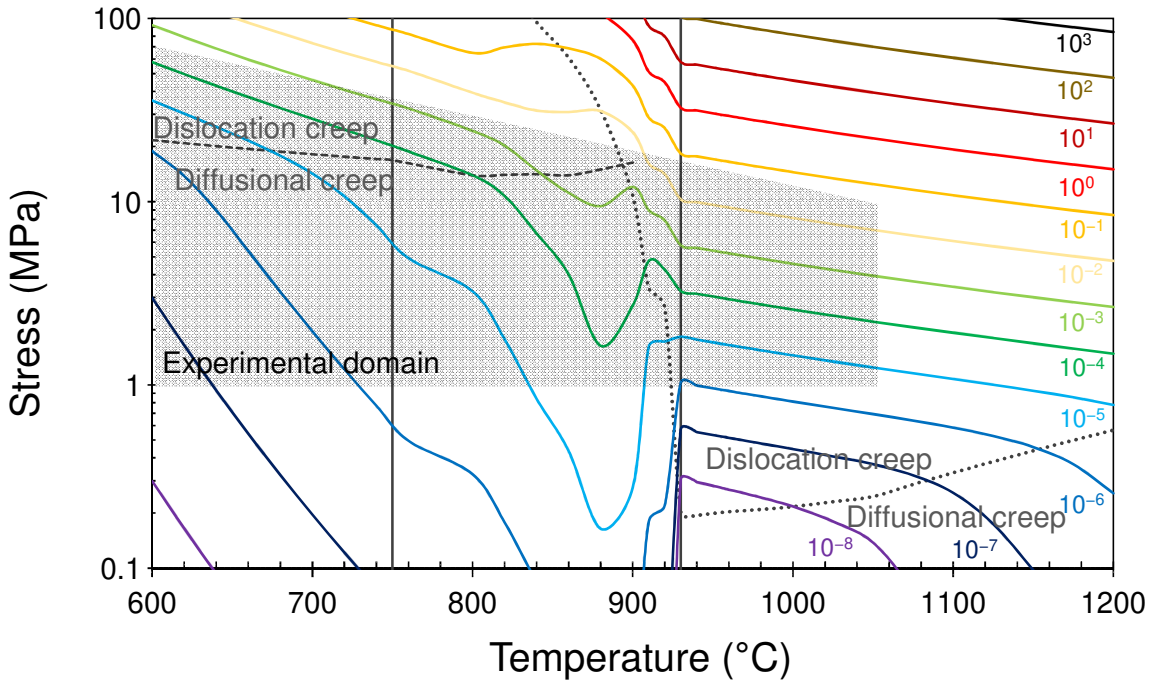

Figure 13: Stress-temperature map with strain rate isovalue curves (in s^{-1}) for $M5_{Framatome}$ alloy – Model predictions, from axial tensile creep tests on sheet specimens (grey region: experimentally investigated domain). Dashed and dotted lines respectively delineate the competition between dislocation creep and diffusional creep regimes for the α and β phases, respectively. Continuous vertical lines delineate boundaries between near-α and (α + β), and (α + β) and full β domains, respectively.

5 Conclusions

Experimental determination of viscoplastic flow of a model $M5_{Framatome}$ sheet, under uniaxial tension in a secondary vacuum, together with simple analytical constitutive modelling led to the following results:

- For the first time, a linear creep regime was evidenced for very low stresses < 10 MPa for the high temperature β phase. It prevails in a very narrow temperature range (900-930°C), in which rapid grain growth of the β phase is inhibited by the small residual fraction of α phase.
- A strong effect of grain size was evidenced in the low-stress creep regime for both α and β phases, together with a limited (Hall-Petch like) effect in the higher stress creep regime for the β phase. The latter effect was not evidenced for the α phase.
- Simple constitutive modelling (multi-mechanism Norton equations taking the grain size into account) together with available viscoplastic homogenisation schemes satisfactorily accounts for experimental observations.
- These results were obtained for uniaxial tension of recrystallized sheets under high vacuum and rather low stresses; further work is still required to explore higher loads levels, different loading modes, environmental conditions and other zirconium alloys.

6 Acknowledgements

This work was co-funded by CEA, EDF and Framatome in the framework of the GAINES project of the French Nuclear Institute I3P. The authors wish to thank Dr N. Richard (Centre des Matériaux) for his help in preparing model near-α microstructures. The help from Dr F. Onimus (CEA) with numerical simulations using the self-consistent homogenisation model is gratefully acknowledged.

7 References

[1] N. Dupin, I. Ansara, C. Servant, C. Toffolon, C. Lemaignan, J.C. Brachet, A thermodynamic database for zirconium alloys, J. Nucl. Mater. 275 (1999) 287-295. https://doi.org/10.1016/S0022-3115(99)00125-7

[2] C. Toffolon-Masclet, J. C. Brachet, C. Servant, J. M. Joubert, P. Barberis, N. Dupin, P. Zeller, Contribution of thermodynamic calculations to metallurgical studies of multi-component zirconium based alloys. J. ASTM Int. 5(7) (2008), 1-21. Paper ID JAI101122. (no doi found)

[3] T.A. Hayes, M.E. Kassner, Creep of zirconium and zirconium alloys, Metall. Mater. Trans. 37A (2006) 2389-2396. https://doi.org/10.1007/BF02586213

[4] I. Charit, K.L. Murty, Creep behavior of niobium-modified zirconium alloys, J. Nucl. Mater. 374 (2008) 354-363. https://doi.org/10.1016/j.jnucmat.2007.08.019

[5] D. Kaddour, S. Fréchinet, A.F. Gourgues, J.C. Brachet, L. Portier, A. Pineau, Experimental determination of creep properties of zirconium alloys together with

phase transformation, Scr. Mater. 51 (2004) 515-519. https://doi.org/10.1016/j.scriptamat.2004.05.046
[6] A. R. Massih, "High-temperature creep and superplasticity in zirconium alloys", J. Nucl. Sci. Technol. 50 (2013) 21-34. https://doi.org/10.1080/00223131.2013.750054
[7] A. J. Ardell (1964). Creep and atomic mobility in polycrystalline zirconium. PhD thesis, Stanford University, CA. (no doi found)
[8] I.M. Bernstein, Diffusion creep in zirconium and certain zirconium alloys, Trans. Metall. Soc. AIME 239 (October 1967) 1518-1522. (no doi found)
[9] R.D. Warda, V. Fidleris, E. Teghtsoonian, Dynamic strain aging during creep of alpha-Zr, Metall. Trans. 4 (1973) 1201-1206. https://doi.org/10.1007/BF02644512
[10] S.R. MacEwen, R.G. Fleck, E.T.C. Ho, O.T. Woo, Deformation of alpha-zirconium in the vicinity of 0.5 T_m, Metall. Trans. A, 12A (1981) 1751-1759. https://doi.org/10.1007/BF02643757
[11] N. Prasad, G. Malakondaiah, P. Rama Rao, Low stress creep behaviour of zirconium, Trans. Indian Institute of Metals 42 (Supplement) (1989), S165-S174. (no doi found)
[12] N. Prasad, G. Malakondaiah, P. Rama Rao, Low stress creep behaviour of Zircaloy-2 vis-a-vis zirconium, Scr. Metall. Mater. 26 (1992) 541-543. https://doi.org/10.1016/0956-716X(92)90280-R
[13] P. Rama Rao, Viscous creep in metals, Current Science 75 (1998) 564-579. (no doi found)
[14] A. T. Donaldson, R. C. Ecob, A transition stress in the creep of an alpha phase zirconium alloy at high temperature, Scr. Metall. 19 (1985) 1313-1318. https://doi.org/10.1016/0036-9748(85)90057-2
[15] G. Malakondaiah, N. Prasad, P. Rama Rao, On the evaluation of activation energy for viscous creep through temperature change tests, Scr. Metall. 16 (1982) 421-426. https://doi.org/10.1016/0036-9748(82)90165-X
[16] J. Fiala, J. Čadek, Creep in zirconium at low stresses and temperatures from 748 to 973 K, Mater. Sci. Eng. 75 (1985) 117-126. https://doi.org/10.1016/0025-5416(85)90183-1
[17] J. Fiala, L. Kloc, J. Čadek, On the low stress creep in Cu-14Al alloy and alpha-zirconium at intermediate temperatures, Mater. Sci. Eng. A136 (1991a) 9-15. https://doi.org/10.1016/0921-5093(91)90437-R
[18] J. Fiala, L. Kloc, J. Čadek, Creep in metals at intermediate temperatures and low stresses: a review, Mater. Sci. Eng. A137 (1991b) 163-172. https://doi.org/10.1016/0921-5093(91)90331-G
[19] B. Kombaiah, K.L. Murty, Coble, Orowan strengthening, and dislocation climb mechanisms in a Nb-modified zircaloy cladding, Metall. Mater. Trans. 46A (2015a) 4646-4660. https://doi.org/10.1007/s11661-015-3060-8
[20] B. Kombaiah, K.L. Murty, High temperature creep and deformation microstructures in recrystallized Zircaloy-4, Philos. Mag. 95 (2015b) 1656-1679. https://doi.org/10.1080/14786435.2015.1042939
[21] D. Campello, N. Tardif, M. Moula, M.C. Baietto, M. Coret, J. Desquines, Identification of the steady-state creep behavior or zircaloy-4 claddings under simulated loss-of-coolant accident conditions based on a coupled experimental/numerical approach, Int. J. Solids Structures 115-116 (2017) 190-199. https://doi.org/10.1016/j.ijsolstr.2017.03.016
[22] A.K. Yadav, C.H. Shin, S.U. Lee, H.C. Kim, Experimental and numerical investigation on thermo-mechanical behavior of fuel rod under simulated LOCA conditions, Nucl. Eng. Des. 337 (2018) 51-65. https://doi.org/10.1016/j.nucengdes.2018.06.023

[23] P. M. Sargent, M. F. Ashby, Deformation maps for titanium and zirconium, Scr. Metall. 16 (1982) 1415-1422. https://doi.org/10.1016/0036-9748(82)90439-2
[24] J. Novotný, J. Fiala, J. Čadek, Harper-Dorn creep in alpha-zirconium, Acta Metall. 33 (1985) 905-911. https://doi.org/10.1016/0001-6160(85)90115-4
[25] T.A. Hayes, M.E. Kassner, R.S. Rosen, Steady-state creep of alpha-zirconium at temperatures up to 850°C, Metall. Mater. Trans. 33A (2002) 337-343. https://doi.org/10.1007/s11661-002-0095-4
[26] M.T. Pérez-Prado, S.R. Barrabes, M.E. Kassner, E. Evangelista, Dynamic restoration mechanisms in alpha-zirconium at elevated temperatures, Acta Mater. 53 (2005) 581-591. https://doi.org/10.1016/j.actamat.2004.10.011
[27] E.A. Abramyan, L.I. Ivanov, N.S. Kudryavtsev, V.A. Yanushkevich, Effect of vacuum on the creep of beta-zirconium at elevated temperatures. Materials Science, 2 (1973) 302-304. (no doi found)
[28] K.M. Rose, E.D. Hindle, The deformation of Zircaloy-2 fuel cladding under loss of coolant accident transients. British Nuclear Energy Society Conference, 1973. (no doi found)
[29] K.M. Rose, E.D. Hindle, Diameter increases in steam generating heavy water reactor zircaloy cans under loss-of-coolant accident conditions, Zirconium in the nuclear industry, ASTM STP 633, eds. A.L. Lowe, Jr, G.W. Parry, ASTM 1977, pp. 24-35. (no doi found)
[30] D.G. Hardy, High temperature expansion and rupture behavior of Zircaloy tubing. American Nuclear Society, Topical Meeting on Water Reactor Safety, 1973, p. 254. (no doi found)
[31] W.R. Clendening, Primary and secondary creep properties for zircaloy cladding at elevated temperatures of interest in accident analyses, Proc. Int. Conf. on Structural mechanics in reactor technology, London, September 1-5, 1975, Ed. T.A. Jaeger, Paper C2/6, North Holland / American Elsevier, pp. 1-9. (no doi found)
[32] C.E.L. Hunt, D.E. Foote, High temperature strain behavior of zircaloy-4 and Zr-2.5Nb fuel sheaths, Zirconium in the nuclear industry, ASTM STP 633, eds. A.L. Lowe, Jr, G.W. Parry, ASTM 1977, pp. 50-65. (no doi found)
[33] B. Burton, G.L. Reynolds, J.P. Barnes, Tensile creep of beta-phase zircaloy-2, J. Nucl. Mater. 73 (1978) 70-76. https://doi.org/10.1016/0022-3115(78)90481-6
[34] B.D. Clay, R. Stride, The creep rupture properties of beta-phase zircaloy-2 cladding in the region 1000-1500°C, Nucl. Eng. Des. 48 (1978) 497-504. https://doi.org/10.1016/0029-5493(78)90093-6
[35] A.S. Rizkalla, R.A. Holt, J.J. Jonas, Effect of oxygen on the deformation of zircaloy-2 at elevated temperatures, Zirconium in the nuclear industry, ASTP STP 681, ASTM 1979, pp. 497-513. (no doi found)
[36] H.E. Rosinger, P.C. Bera, W.R. Clendening, Steady-state creep of zircaloy-4 fuel cladding from 940 to 1873 K, J. Nucl Mater. 82 (1979) 286-297. https://doi.org/10.1016/0022-3115(79)90011-4
[37] R.S.W. Shewfelt, L.W. Lyall, D.P. Godin, A high-temperature creep model for Zr-2.5 wt% Nb pressure tubes, J. Nucl. Mater. 125 (1984) 228-235. https://doi.org/10.1016/0022-3115(84)90548-8
[38] M. Stephan, E. Adam, L. Wetzel, Activation energies for thermal creep of the Zr1%Nb alloy in the alpha-Zr and beta-Zr phase regions, Kerntechnik 57 (1992) 129-132. https://doi.org/10.1515/kern-1992-570221
[39] S. Fréchinet, Transformations and behaviours of zircaloy-4 in anisothermal conditions, Ph.D. thesis, Ecole des Mines de Paris, Paris, France, 2001 (in French).

[40] D. Kaddour, Isothermal and anisothermal creep of an Zr-1%Nb alloy in the single-phase (alpha and beta) and two-phase (alpha + beta) domains, Ph.D. thesis, Ecole des Mines de Paris, Paris, France, 2004, available from http://tel.archives-ouvertes.fr/tel-00162151 (in French)
[41] B.S. Rodchenkov, A.N. Semenov, High temperature mechanical behavior of Zr-2.5% Nb alloy, Nucl. Eng. Des. 235 (2005) 2009-2018. https://doi.org/10.1016/j.nucengdes.2005.05.032
[42] M.I. Alymov, E.N. Pigorov, L.L. Artyukhina, O.V. Komarov, N-1 alloy creep at 1170-1370K, Soviet Atomic Energy 65 (1987) 791-792. https://doi.org/10.1007/BF011230
[43] D. Lee, W.A. Backofen, Superplasticity in some titanium and zirconium alloys, Trans. Metall. Soc. AIME 239 (1967) 1034-1040. (no doi found)
[44] H.M. Chung, A.M. Garde, T.F. Kassner, Deformation and rupture behavior of zircaloy cladding under simulated loss-of-coolant accident conditions, Zirconium in the Nuclear Industry, ASTM STP 633, eds. A.L. Lowe, Jr, G.W. Parry, ASTM, 1977, pp 82-97. https://doi.org/10.1520/STP35566S
[45] R.N. Singh, R. Kishore, T.K. Sinha, B.P. Kashyap, Superplastic behaviour of a Zr-2.5 wt% Nb pressure tube alloy, Scr. Metall. Mater. 28 (1993) 937-942. https://doi.org/10.1016/0956-716X(93)90059-2
[46] R. Fotedar, R. Kishore, B.P. Kashyap, S. Banerjee, Superplastic forming of zircaloy-2 pressure tube material, Mater. Sci. Forum 243-245 (1997) 663-668. https://doi.org/10.4028/www.scientific.net/MSF.243-245.663
[47] S.V. Shukla, C. Chandrashekharayya, R.N. Singh, R. Fotedar, R. Kishore, T.K. Sinha, B.P. Kashyap, Effect of strain rate and test temperature on superplasticity of a Zr-2.5 wt% Nb alloy, J. Nucl. Mater. 273 (1999) 130-138. https://doi.org/10.1016/S0022-3115(99)00037-9
[48] P.S. Hill, N. Ridley, R.I. Todd, Investigation of superplastic behaviour and solid state bonding of zircaloy-4, Mater. Sci. Forum 357-359 (2001) 99-104. https://doi.org/10.4028/www.scientific.net/MSF.357-359.99
[49] R.N. Singh, R. Kishore, A.K. Singh, T.K. Sinha, B.P. Kashyap, Microstructural instability and superplasticity in a Zr-2.5 wt% Nb pressure tube alloy, Metall. Mater. Trans.32A (2001) 2827-2840. https://doi.org/10.1007/s11661-001-1033-6
[50] R. Kapoor, J.K. Chakravartty, C.C. Gupta, S.L. Wadekar, Characterization of superplastic behaviour in the (alpha + beta) phase field of Zr-2.5 wt% Nb alloy, Mater. Sci. Eng. A392 (2005) 191-202. https://doi.org/10.1016/j.msea.2004.09.023
[51] A. Saboori, M. Dadkhah, M. Pavese, D. Manfredi, S. Biamino, P. Fino, Hot deformation behavior of Zr-1%Nb alloy: flow curve analysis and microstructure observations, Mater. Sci. Eng. A696 (2017) 366-273. https://doi.org/10.1016/j.msea.2017.04.049
[52] A. Sarkar, S.A. Chandanshive, M.K. Thota, R. Kapoor, High temperature deformation behavior of Zr-1Nb alloy, J. Alloys Compounds 703 (2017) 56-66. https://doi.org/10.1016/j.jallcom.2017.01.356
[53] K.K. Saxena, K.S. Suresh, R.V. Kulkarni, K.V. Mani Krishna, V. Pancholi, D. Srivastava, Hot deformation behavior of Zr-1Nb alloy in two-phase region - microstructure and mechanical properties, J. Alloys Compounds 741 (2018) 281-292. https://doi.org/10.1016/j.jallcom.2018.01.008
[54] R.S.W. Shewfelt, L.W. Lyall, A high-temperature longitudinal strain rate equation for Zr-2.5 wt% Nb pressure tubes, J. Nucl. Mater. 132 (1985) 41-46. https://doi.org/10.1016/0022-3115(85)90391-5
[55] T. Jailin, N. Tardif, J. Desquines, P. Chaudet, M. Coret, M.-C. Baietto, V. Georgenthum, Thermo-mechanical behavior of zircaloy-4 claddings under simulated

post-DNB conditions, J. Nucl. Mater. (2020) paper 151984. https://doi.org/10.1016/j.jnucmat.2020.151984
[56] E. Adam, B. Hallau, L. Wetzel, Untersuchungen zum sekundären Kriechverhalten von Brennelementhüllrohren as ZrNb1 unter Extresbelastungen, Kernenergie 28 (1985) 233-236 (in German).
[57] E. Adam, M. Stephan, L. Wetzel, Dehnverhalten von ZrNb1-Brennelementhüllrohren eines WWER-Reaktors beim Kühlmittelverluststörfall, Kernenergie 30 (1987) 382-384 (in German).
[58] E. Adam, M. Stephan, L. Wetzel, Kriechverhalten von ZrNb1-Brennelementhüllrohren in Argon and Wasserdampf, Kernergie 31 (1988) 461-464 (in German).
[59] E. Adam, M. Stephan, L. Wetzel, Standzeit von ZrNb1-Brennelementhüllrohren unter Störfallbedingungen, Kerntechnik 54 (1989) 169-172 (in German).
[60] M.E. Kassner, P. Kumar, W. Blum, Harper-Dorn creep, Int. J. Plast. 23 (2007) 980-1000. https://doi.org/10.1016/j.ijplas.2006.10.006
[61] D. Kaddour, A.-F. Gourgues-Lorenzon, J.C. Brachet, L. Portier, A. Pineau, Microstructural influence on high temperature creep flow of Zr-1%Nb(O) alloy in near-alpha, (alpha + beta), and beta temperature ranges, J. Nucl. Mater. 408 (2011) 116-124. https://doi.org/10.1016/j.jnucmat.2010.11.025
[62] R. Chosson, A.F. Gourgues-Lorenzon, V. Vandenberghe, J.C. Brachet, J. Crépin, Creep flow and fracture behavior of the oxygen-enriched alpha phase in zirconium alloys, Scr. Mater. 117 (2016) 20-23. https://doi.org/10.1016/j.scriptamat.2016.02.021
[63] J.P. Langeron, P. Lehr, Etude de la transformation allotropique alpha / beta du zirconium, Mem. Sci. Rev. Metall. 56 (1959) 307-315 (in French). (no doi found)
[64] A. Nowikov, I. Pfeiffer, Schmeltzen, Verarbeitung and mechanische Eigenschaften von Zircaloy-2, Z. Metallkunde 48 (1957) 479-483 (in German). https://doi.org/10.1515/ijmr-1957-480811
[65] H.E. Sills, R.A. Holt, Predicting high-temperature transient deformation from microstructural models, Zirconium in the nuclear industry, ASTP STP 681, ASTM 1979, pp. 325-341. https://doi.org/10.1520/STP36688S
[66] http://www-cast3m.cea.fr (accessed on 28. September, 2021)
[67] K. L. Murty, J. Ravi, Wiratmo, Transitions in creep mechanisms and creep anisotropy in Zr - 1Nb - 1Sn - 0.2Fe sheet, Nucl. Eng. Des. 156 (1995) 359-371. https://doi.org/10.1016/0029-5493(94)00960-7
[68] K.L. Murty, G. Dentel, J. Britt, Effect of temperature on transitions in creep mechanisms in class-A alloys, Mater. Sci. Eng. A410-411 (2005) 28-31. https://doi.org/10.1016/j.msea.2005.08.006
[69] Y. Zhou, B. Devarajan, K.L. Murty, Short-term rupture studies of zircaloy-4 and Nb-modified Zircaloy-4 tubing using closed-end internal pressurization. Nucl. Eng. Des. 228 (2004) 3-13. https://doi.org/10.1016/j.nucengdes.2003.06.013
[70] T.R.G. Kutty, T. Jarvis, C. Ganguly, Hot hardness and indentation creep studies on Zr - 1Nb - 1Sn - 0.1Fe alloy, J. Nucl. Mater. 246 (1997) 189-195. https://doi.org/10.1016/S0022-3115(97)00108-6
[71] P. Shahinian, J.R. Lane, Influence of grain size on high-temperature properties of monel. Transactions of the Metallurgical Society of the American Institute of Mining, Metallurgical, and Petroleum Engineers, 45 (1953) 177-199. (no doi found)
[72] F. Garofalo, W.F. Domis, F. von Gemmingen. Effect of grain size on the creep behavior of an austenitic iron-base alloy. Transactions of the Metallurgical Society of the American Institute of Mining, Metallurgical, and Petroleum Engineers 230 (1964) 1460-1467. (no doi found)

[73] R. A. Petkovic, M. J. Luton, J. J. Jonas. Grain size and high-temperature yield strength of polycrystalline copper. Metal Science 13 (1979) 569-572. https://doi.org/10.1179/030634579790434088

[74] M. E. Kassner, X. Li. The effect of grain size on the elevated temperature yield strength of polycrystalline aluminum. Scr. Metall. Mater. 25 (1992) 2833-2838. https://doi.org/10.1016/0956-716X(91)90165-W

[75] G. Trego, High temperature creep behaviour of the M5® alloy in the (alpha + beta) two-phase domain, Ph.D thesis, MINES ParisTech, 2011, Paris, France, available from http://pastel.archives-ouvertes.fr/pastel-00688207 (in French).

[76] J. Qu, M. Cherkaoui, Fundamentals of micromechanics of solids, Wiley, Hoboken, New Jersey, USA, 2006. ISBN: 978-0-471-46451-8

[77] P. Ponte Castañeda, Second-order homogenization estimates for nonlinear composites incorporating field fluctuations. I-Theory. J. Mech. Phys. Solids 50 (2002a) 737-757. https://doi.org/10.1016/S0022-5096(01)00099-0

[78] P. Ponte Castañeda, Second-order homogenization estimates for nonlinear composites incorporating field fluctuations. II-Applications. J. Mech. Phys. Solids 50 (2002b) 759-782. https://doi.org/10.1016/S0022-5096(01)00098-9

[79] R. Brenner, O. Castelnau, and L. Badea (2004) Mechanical field fluctuations in polycrystals estimated by homogenization techniques, Proc. R. Soc. Lond. A 46035893612, doi:10.1098/rspa.2004.1278

[80] P. Pilvin, F. Onimus, R. Brenner, S. Pascal, X. Feaugas, K. Saï, Finite element assessment of an affine self–consistent model for hexagonal polycrystals, European Journal of Mechanics A/Solids 61 (2017) 345-356. https://doi.org/10.1016/j.euromechsol.2016.10.010

[81] O. Castelnau, D. K. Blackman, R. A. Lebensohn, and P. Ponte Castaneda, Micromechanical modeling of the viscoplastic behavior of olivine, J. Geophys. Res. 113 (2008) B09202, doi:10.1029/2007JB005444.

[82] T. Kanit, S. Forest, I. Galliet, V. Mounoury and D. Jeulin, Determination of the size of the Representative Volume Element for random composites: statistical and numerical approach, International Journal of Solids and Structures 40 (2003) 3647-3679. https://doi.org/10.1016/S0020-7683(03)00143-4

[83] L. Darchis, P. Lemoine, Modélisation de la déformation de gaines en zircaloy dans des conditions d'un accident de perte de réfrigérant primaire : critère de rupture, Technical report, CEA Saclay, 1984 (in French).